73W-00271

PREPARED FOR THE

GEORGE C. MARSHALL SPACE FLIGHT CENTER

HUNTSVILLE, ALABAMA

CONTRACT NO. NAS8-14000

S/A 2171, TD 0343-73

UCN 15597

IBM REPORT NO. 73W-00271

SEPTEMBER 1973

DYNAMIC CHARACTERIZATION OF SOLID ROCKETS

IBM, FEDERAL SYSTEMS DIVISION, ELECTRONICS SYSTEM CENTER

HUNTSVILLE, ALABAMA

ABSTRACT

This report describes a study task dealing with the structural dynamics of solid rockets. The method used in gaining background material and the use of this material in evaluating the structural dynamics of the SRB are described. Propellant modes which are self-excited are analyzed in detail. The necessity of testing propellant modes is established and the requirements for this test are described.

TABLE OF CONTENT

TABLE OF CONTENTS (CONT'D)

TABLE OF CONTENTS (CONT'D)

ACKNOWLEDGEMENTS

We wish to acknowledge the information obtained from Mr. Thomas Duerr, Chief of Propulsion Mechanics, Propulsion Directorate, U.S. Army Missile Command. The information relating to his experience with regards to dynamic problems in solid rocket motor development, instilled in us early in the study the fact that the properties of the propellant are beneficial with regards to structural dynamics since solid propellant is a highly damped material.

We also wish to acknowledge the information obtained from Mr. George Stibor of TCC who is with the Wasatch Division, Brigham City, Utah. Mr. Stibor's willingness to volunteer information was most helpful in obtaining information and applicable technical papers.

SYMBOLS AND UNITS

a = bore radius of propellant core

A_c = area of normal cross-section of motor case (in^2)

A_p = area of normal cross-section of propellant $(in)^2$

b = outer radius of propellant core (in)

c = viscous damping constant (#sec/in) or speed of sound in chamber gases (in/sec)

c_c = critical damping constant (# sec/in)

C_1, C_2 = arbitrary constants

E_c = modulus of elasticity of case (psi)

E_p = modulus of elasticity of propellant (psi)

E' = storage modulus (real part of complex elastic modulus) psi

E'' = loss modulus (imaginary part of complex elastic modulus) psi

f = frequency (Hertz)

$F_{t\ allowable}$ = allowable tensile strength (psi)

F_{tu} = ultimate tensile strength (psi)

g = gravitational constants or $\left[K''\right] / \left[K'\right] = \tan\theta$ (section 4.3.2 only)

G = shear modulus or modulus of rigidity (psi)

G' = real part of complex shear modulus (psi)

G'' = imaginary part of complex shear modulus (psi)

h = thickness of motor case (in)

i = $\sqrt{-1}$

I_c = area moment of inertia of motor case (in^4)

I_p = area moment of inertia of propellant case (in^4)

J_o = zero order Bessel function of the first kind

J_1 = first order Bessel function of the first kind

K = discontinuity factor or spring constant (section 4.3.2 only)

K' = real part of complex spring constant (section 4.3.2 only)

K'' = imaginary part of complex spring constant (section 4.3.2 only)

L = length (in)

m = tangential wave number for acoustic modes or frequency number

M = actual mass

$\bar{M}$ = equivalent mass for constant kinetic energy system

n = radial wave number for acoustic modes or mode number

p = pressure (psi)

q = longitudinal wave number for acoustic modes

r = radial coordinate

R_o = bore radius of propellant core (in)

R_1 = inside radius of motor case (in)

R_2 = outside radius of motor case (in)

R_c = mean radius of motor case (in)

s, s* = scale factors

S.F. = safety factor

t = time

u_r = radial displacement

u_θ = circumferential displacement

u_z = axial displacement

W = $W(r)$ function r only

Y_o = zero order Bessel function of the second kind

Y_1 = first order Bessel function of the second kind

Z = axial coordinate

α = $\frac{w_n}{2}\left\{(1+g^2)^{1/2}-1\right\}^{1/2}$ (section 4.3.2 only)

α_{mn} = characteristic value of tranverse wave (m, n)

γ = density (#/in^3)

$\gamma_{r\theta}, \gamma_{rz}, \gamma_{\theta z}$ = shear strains

Δ = cubical dilation = $\partial u_r/\partial r + u_r/r + (1/r)(\partial u_\theta/\partial \theta) + \partial u_z/\partial z$

$\varepsilon_r, \varepsilon_\theta, \varepsilon_z$ = normal strains in the radial, circumferential and axial

ζ = c/c_c

θ = circumferential coordinate

ν = Poisson's ratio

ρ = mass density = γ/g (#sec^2/in^4)

$\sigma_r, \sigma_\theta, \sigma_z$ = normal stresses

$\tau_{r\theta}, \tau_{rz}, \tau_{\theta z}$ = shear stresses

ω = circular frequency or $\frac{\omega_n}{2}\left\{(1+g^2)^{1/2}+1\right\}^{1/2}$ (section 4.3.2 only)

Ω_m = circular frequency coefficient for the m the mode

∇^2 = Laplacian = $\partial^2/\partial r^2 + (1/r)(\partial/\partial r) + (1/r^2)(\partial^2/\partial\theta^2) + \partial^2/\partial z^2$

1.0 INTRODUCTION

This report describes a technical study task which deals with the structural dynamics of solid rockets. The scope of the task was to first determine the dynamic properties of solid propellant such as PBAN and then to determine the dynamic characteristics of a solid booster for which analysis and/or test would be required in a solid booster stage development program. The task was performed for the Structural Dynamics Section, Analytical Mechanics Division, Astronautics Laboratory, Science and Engineering Directorate, Marshall Space Flight Center, National Aeronautics and Space Administration.

During the initial phases of this study, a literature search was conducted to obtain reference material related to the structural dynamics of solid rockets including material properties of the propellant. Many applicable papers and handbooks were located and are referenced in the bibliography. Those references in the bibliography which are of particular interest are abstracted.

Concurrently with the literature search, inquiries were made to U. S. Army and contractor experts to obtain reference material on structural dynamics of solid rockets and to determine what, if any, type of dynamic problems have been encountered in solid rocket development.

At Redstone Arsenal, U. S. Army Missile Command, the Propulsion Directorate (AMSMI-RK) was contacted. It was ascertained that there are no case histories of dynamic problems related to Army solid rocket development wherein the dynamics during burn are involved. Where the rockets are subjected to transportation environments for considerable time before use, fatigue in the propellant grain design must be considered.

Two contractors, namely Thiokol Chemical Corporation (TCC) and United Technology Center (UTC) were contacted. At TCC, information related to experience with Minuteman First Stage and other solid rocket motor development was obtained. This information included the following:

(1) Minuteman First Stage test reports
(2) Several papers related to modal frequency analysis
(3) Dynamic properties of PBAN (Polybutadiene-acrylic acid-acrylonitrile terpolymer)

At UTC information related to the following was obtained:

(1) Dynamics related to thrust termination
(2) Effects of propellant on bending modes
(3) Dynamic properties of PBAN propellant

During the study a review of the dynamic properties of a solid propellant was made. Since solid propellant is a viscoelastic material, the theory for a viscoelastic material and its dynamic properties are developed in Appendix A. Because PBAN is most apt to be used in future development of the solid motor for the Space Shuttle, its properties are studied and are presented in Section 2.3.

A review was made of various modes of vibration that can exist for a solid propellant rocket and are discussed in Section 3. Of all the various vibration modes studied, the study of the Fundamental Axisymmetric Longitudinal Thickness Shear Modes received the most attention. The reasons for interest in this mode are as follows:

(1) It may occur at approximately 18 Hertz which is in the frequency range of interest (0-30 Hz).
(2) It depends only on the density, dynamic shear modulus and the inside-outside diameters of the propellant core.
(3) It can be excited by the longitudinal (closed-closed) motor chamber acoustic mode.
(4) The dynamic shear modulus varies with temperature, pressure, frequency and strain level. Specific shear modulus data for the service conditions of the rocket motor to be analyzed is therefore necessary.

Extensive analysis of the longitudinal thickness shear mode is described in Section 4. Both theoretical solutions and NASTRAN computer model solutions were obtained to show effects of high and low modulus, high and low strain and real vs complex modulus. Analysis was also performed to evaluate length and size effects on a test segment.

Dynamic testing of the total Shuttle vehicle in the lift-off configuration is considered a necessary requirement to evaluate the complex total vehicle dynamic analysis. Dynamic testing of the individual SRB stage for those modes involving the SRB structure would therefore not be considered practical because of the difficulty of simulating the motion restraints which are introduced by the External Tank and Orbiter. Propellant modes, namely the Lobar and Longitudinal Thickness Shear Modes, would not however be affected by these restraints and could be

evaluated by individual SRB Stage tests. Furthermore, both of these modes could be evaluated by a SRB segment test. Because excitation of the Fundamental Axisymmetric Longitudinal Thickness Shear Mode by the motor chamber closed-closed acoustic mode is expected, and also because of the difficulty of identifying the dynamic shear modulus as discussed in (4) above, segment level listing of the Fundamental Axisymmetric Longitudinal Thickness Shear Mode is considered necessary. Requirements for this test are described in Appendix C.

Although no particular detrimental effects are expected from excitation of the Fundamental Axisymmetric Longitudinal Thickness Shear Mode of vibration, its frequency and therefore time of occurrence are difficult to predict precisely. The feasibility of a segment test and the requirement for a test to verify analysis were established during this study. It is therefore recommended that a segment test be conducted as early as possible in the SRB development program.

2.0 PHYSICAL DESCRIPTION OF SRB

2.1 Introduction

The particular solid rocket motor studied is the Solid Rocket Booster (SRB) proposed for the Space Shuttle. The physical size and other parameters for this booster were obtained from MSFC-S&E-ASTN-PE. At the time the SRB parameters were obtained, the development was in the conceptual design phase and therefore subject to change. The design studied consisted of a high strength steel case with an outside diameter of 142 inches and a length of 1325 inches. The rocket will be composed from three to five segments. The propellant, with a circular bore of 40 inch diameter, will be poured into each segment. The internal pressure will be 1000 psi during combustion.

2.2 SRB Cast Definition

The case material is high strength steel, D6AC, which has an ultimate strength of 195,000 psi. Using a safety factor of 1.4 and a discontinuity factor of 1.2 the wall thickness can be calculated using the following equations:

$$F_{t\ allowable} = \frac{F_{tu}}{S.F.} \qquad (1)$$

and

$$F_{t\ allowable} = \frac{K\ p\ R_1}{h} \qquad (2)$$

Combining equations the wall thickness is

$$h = \frac{KpR_1S.F.}{F_{tu}} \qquad (3)$$

or

$$h = 0.612 \text{ inches} \qquad (4)$$

2.3 Core Material Properties

The propellant used in the study is PBAN (Poly butadiene-acrylic acid-acrylonitrile terpolymer) which is a viscoelastic material. It contains 86% solids and 16% aluminum, has an operating temperature range of 30 to 90°F and density of 0.064 pounds per cubic inch. The properties of viscoelastic materials in general are discussed in Appendix A and the properties of PBAN in particular are discussed in this section.

2.3.1 Poisson's Ratio

In Section 2.0 of Appendix A, it is shown that the Poisson's ratio for viscoelastic materials is 0.5. This leads to problems when using existing computer codes due to the presence of a 1-2 ν term in the denominator. The handling of this problem varies with contractors. Thiokol Chemical Corporation uses a value of 0.495 and United Technology Center rewrites their computer codes to accept 0.5. It is interesting to note that in the development of the equations of the thickness shear vibration mode (Section 4.2) the 1-2 ν term in the denominator drops out.

2.3.2 Elastic Modulus Shear Modulus

In Section 3.0 of Appendix A, it is shown that the elastic modulus and shear modulus for viscoelastic materials are complex quantities that vary with strain, frequency, pressure, and temperature. The effects of temperature can be disregarded due to the low thermal conductivity and the high burning rate of the propellant. The increase in pressure causes an increase in modulus, therefore, since the interest is in low frequencies, it will be conservative to use the modulus for atmospheric pressure. The effects of strain and frequency should be included in a modal analysis of a viscoelastic material. It was shown in Section 3.0 of Appendix A that the moduli increase with a decrease in strain. During the contacts with the propellant manufacturers the shear modulus for both high and low strains were obtained. The shear moduli for low strains was obtained from UTC and is shown in Figure 2-1. The equation for the shear storage modulus for low strains can be expressed as a function of frequency. It is

$$G' = 2800\ f^{0.220} \qquad (5)$$

The shear moduli for high strains was obtained from TCC and is shown in Figure 2-2. The equation for the shear storage modulus for high strain is

$$G' = 900\ f^{0.145} \qquad (6)$$

It is seen that there is a large spread in the shear moduli for high and low strains. It is therefore evident that it is important to determine the strain levels in the propellant and the shear modulus at that strain.

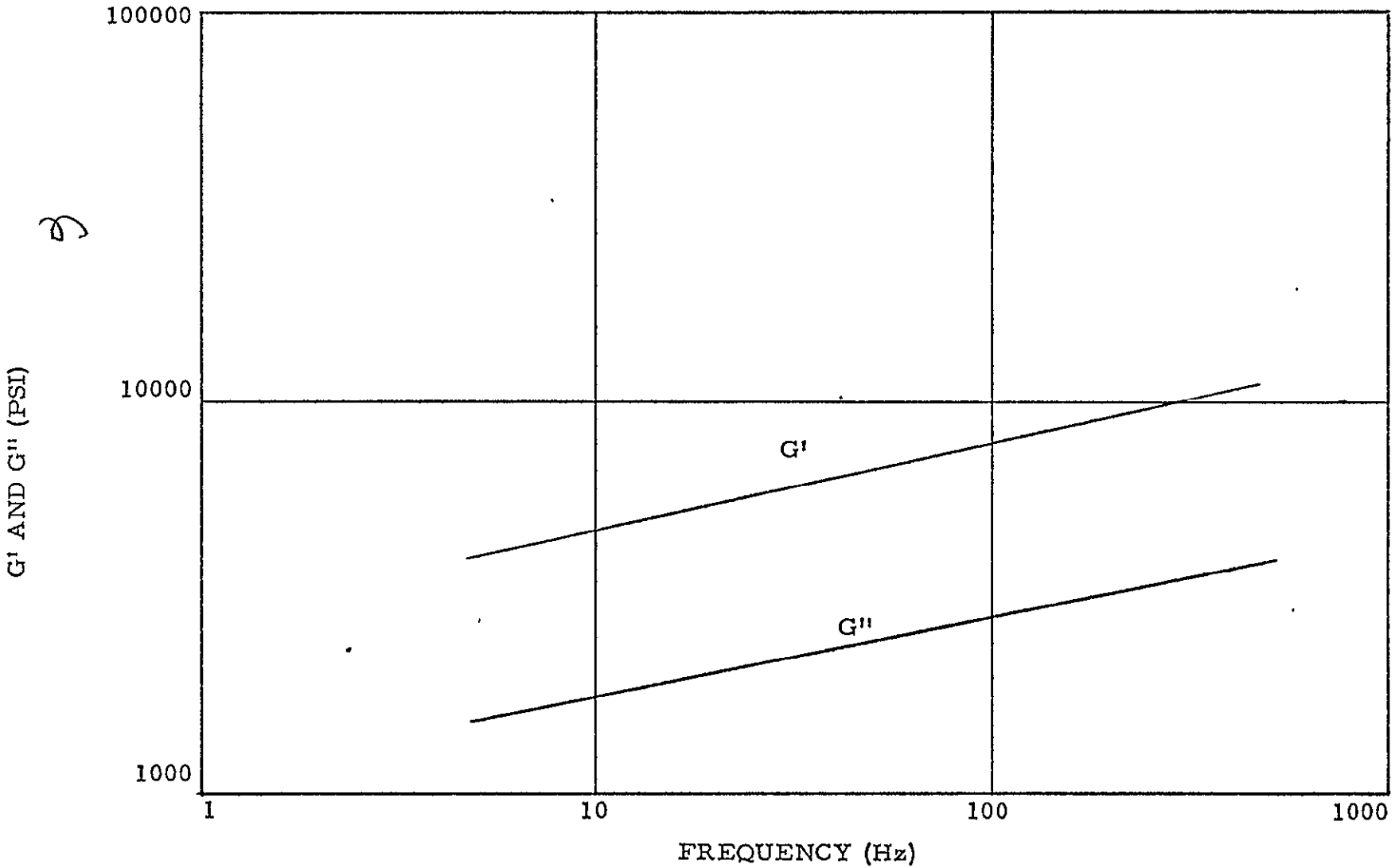

Figure 2-1. Dynamic Shear Moduli for Low Strains

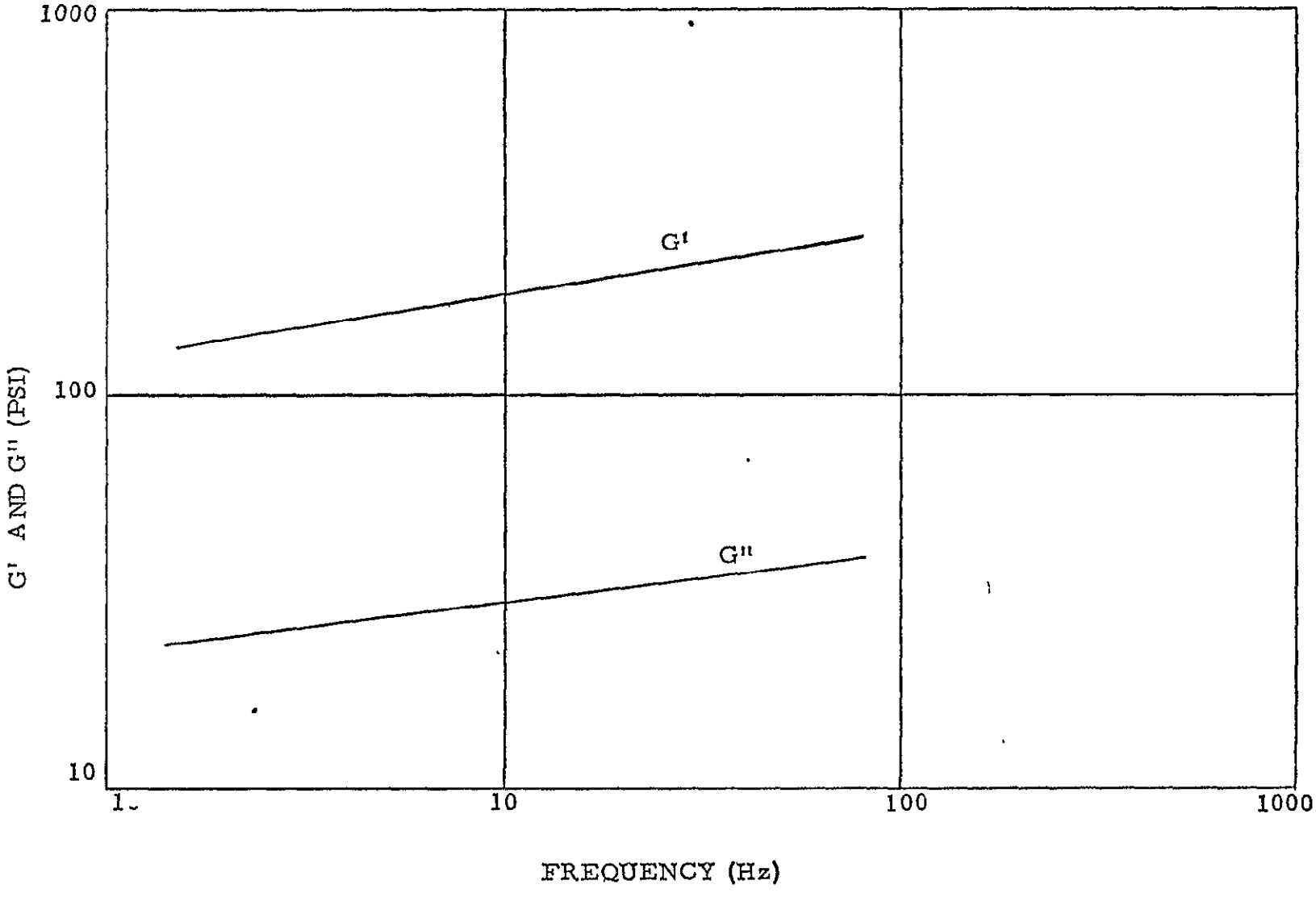

Figure 2-2. Dynamic Shear Moduli for High Strains

2.3.3 Damping Ratio

In Section 3.0 of Appendix A, it is shown that the damping ratio is given by

$$\zeta = \frac{c}{c_c} = \frac{E''}{2E'}$$

The damping ratio for low strain can be found from Figure 2-1. It is 0.18 in the frequency range of interest (10-50 hertz). The damping ratio for high strain can be found from Figure 2-2. It is 0.12 in the frequency range of interest (10-50 hertz). The damping ratio for both high and low strains is high, therefore, the propellant modes will be hard to excite and the propellant will act as an energy sink.

3.0 STRUCTURAL DYNAMICS OF A SOLID ROCKET

3.1 Introduction

A general objective for this work was to define the dynamics which are related to the interaction between structure and propellant. Since the modulus of solid propellant varies with so many parameters, the modes which result from resonance within the propellant were considered to be those to which this study should focus. These modes are the lobar (breathing) and longitudinal thickness shear modes. When considering the possibility of coupling of these modes with total Shuttle Vehicle vibration, the longitudinal thickness shear is the most significant. Particular emphasis was therefore placed on this mode. During the study, however, reference material was obtained on the vibration analysis of the solid rocket in general. In order to present this information for future reference, other possible modes of vibration will also be briefly discussed in this section.

3.2 Bending Modes

Most applications of a solid rocket would require analysis for the clamped-free and free-free bending modes. The mode shapes for these modes are illustrated in Figure 3-1 for simple beams and can be found in most texts on vibrations of beams. The clamped-free bending modes would exist prior to release and the free-free bending modes could exist after release. The free-free modes of course continually change with the decrease in mass as the propellant is consumed.

The pre-release bending modes of the Solid Rocket Booster for the Space Shuttle are more complex than the case described above. The two Solid Rocket Boosters (SRB) in one concept are attached to the External Tank fore and aft at stations 404 and 1515. The forward attachment points can transfer direct loads only to the External Tank. The aft attachment points are a sliding joint in the longitudinal direction. Direct loads in the radial and lateral directions and local bending moments are transferred by these joints to the External Tank. Figures 3-2 illustrates a simple model of the Space Shuttle for the lift-off configuration. The inflight model would be the same except the restraints at the base of the SRBs would be removed. No analysis of the Space Shuttle configuration was performed because it was not in scope. It can be seen from the above discussion that dynamic testing to evaluate the bending modes of the SRB would have to be performed on a total Solid Rocket Booster/External Tank/Orbiter Configuration.

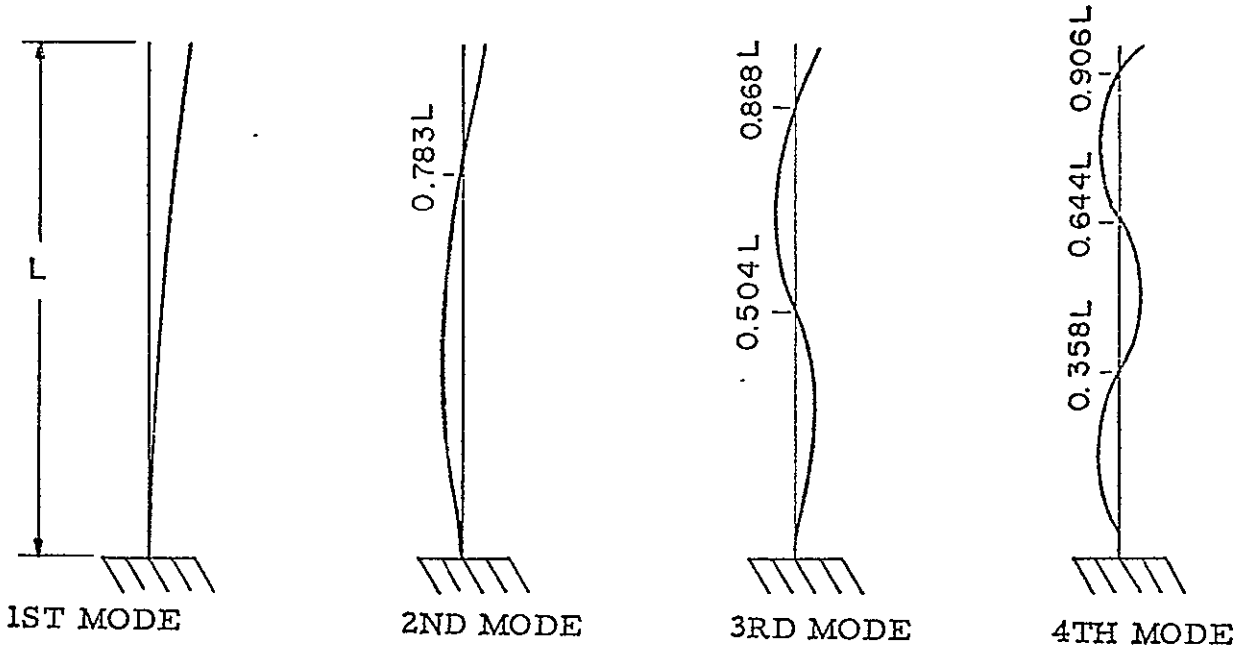

CLAMPED-FREE

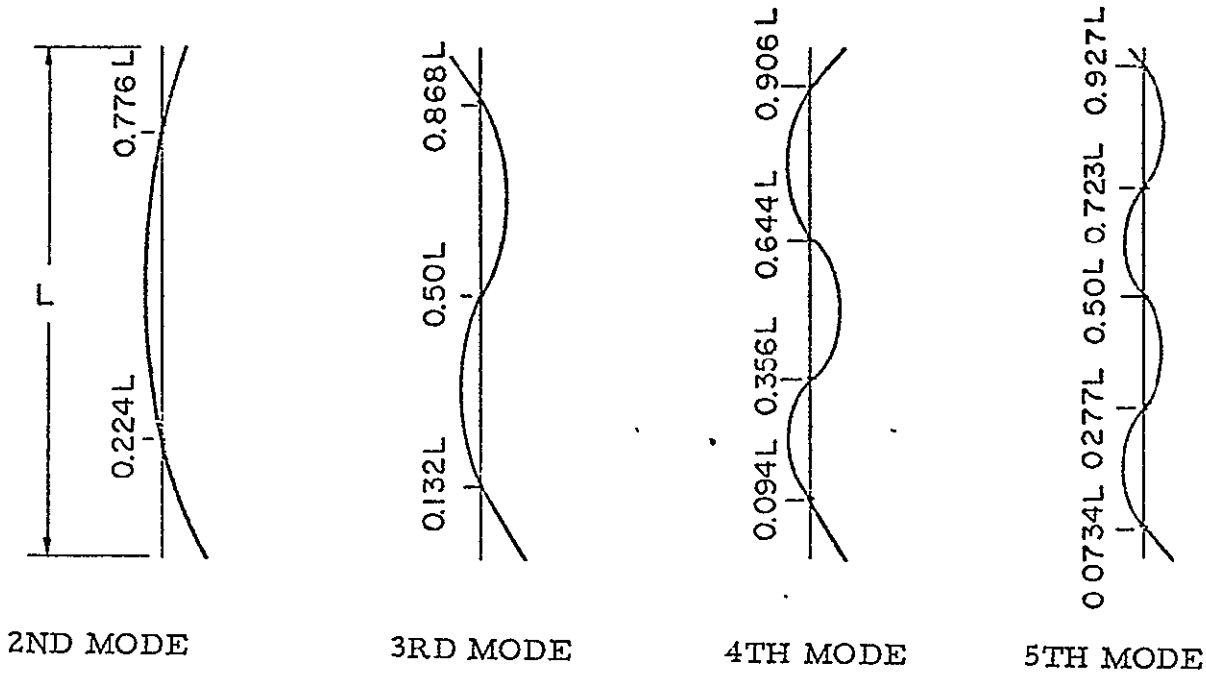

FREE-FREE

Figure 3-1. Bending Mode Shapes

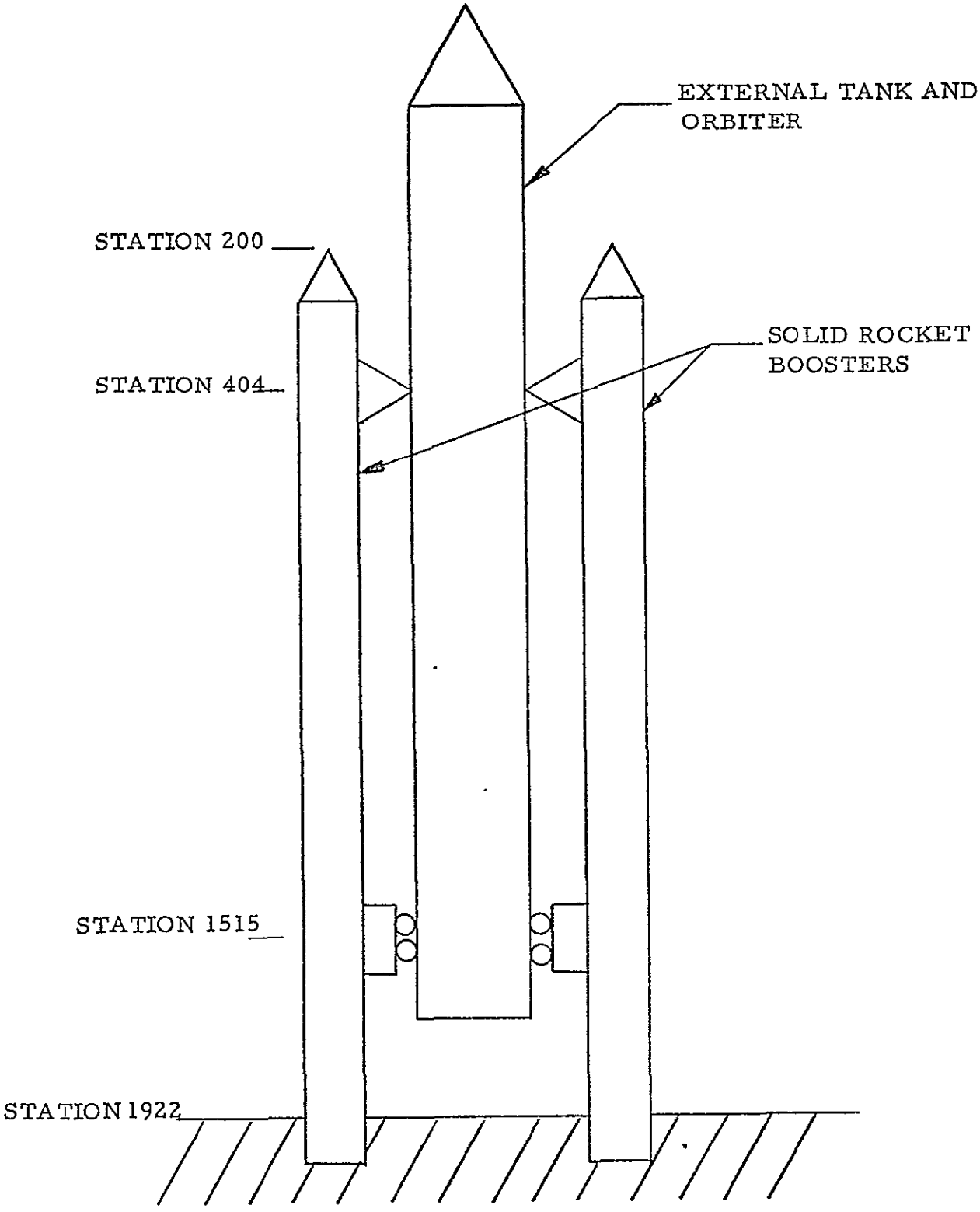

Figure 3-2. SRB Lift-Off Model

It is significant to note that the properties of the propellant have little effect on the stiffness of a solid rocket in bending. This can be seen by examining the (EI) terms for the case and propellant in Table 3-1 for the SRB.

Note that the EI term for the total stage cross-section is only 1/2% greater than the case itself. Therefore the case stiffness is seen to dominate the total rocket stiffness for any analysis.

Section	O.D.	I.D.	I	E	EI
Case	142 in	141 in	$.5563 \times 10^{6}$ in^4	28×10^{6} psi	1.558×10^{13} #in^2
Propellant	141 in	40 in	$.1928 \times 10^{8}$ in^4	4000 psi	$.008 \times 10^{3}$ #in^2
Case & Propellant	—	—	—	—	1.566×10^{3} #in^2

Table 3-1. SRB Stiffness Terms

The free-free fundamental bending mode for a solid rocket can be calculated by a method described in Reference 18. The solution assumes a rocket to be a moderately thick beam and therefore includes the effects of transverse shear deformation and rotary inertia. The reference solves for the fundamental frequency of a solid rocket having similar parameters to the SRB. Solution of these equations are very complex and therefore the fundamental bending mode of the SRB was not calculated. The solution of the example problem in Reference 18 is shown below since it illustrates the method used. Figure 3-3 shows the effective geometric parameters required in the solution.

$$2-2 \quad \text{Cosh } \gamma L \text{Cos } \delta L + \left[\frac{\gamma(\chi+\gamma^2)}{\delta(\chi-\delta^2)} - \frac{\delta(\chi-\delta^2)}{\gamma(\chi+\gamma^2)}\right] \text{Sinh } \gamma L \text{ Sin } \delta L = 0$$

where

$$\chi = \frac{2(\gamma A)_T \omega^2}{g G_c A_c}, \quad \gamma^2 = \beta - \alpha, \quad \delta^2 = \beta + \alpha$$

$$\alpha = \frac{\omega^2}{2}\left[\frac{2(\gamma A)_T}{g G_c A_c} + \frac{(\gamma I)_T}{g E_c I_c}\right]$$

$$\beta = \frac{1}{2}\left\{\frac{4(\gamma A)_T \omega^2}{g E_c I_c} + \omega^4\left[\frac{2(\gamma A)_T}{g G_c A_c} - \frac{(\gamma I)_T}{g E_c I_c}\right]^2\right\}^{1/2}$$

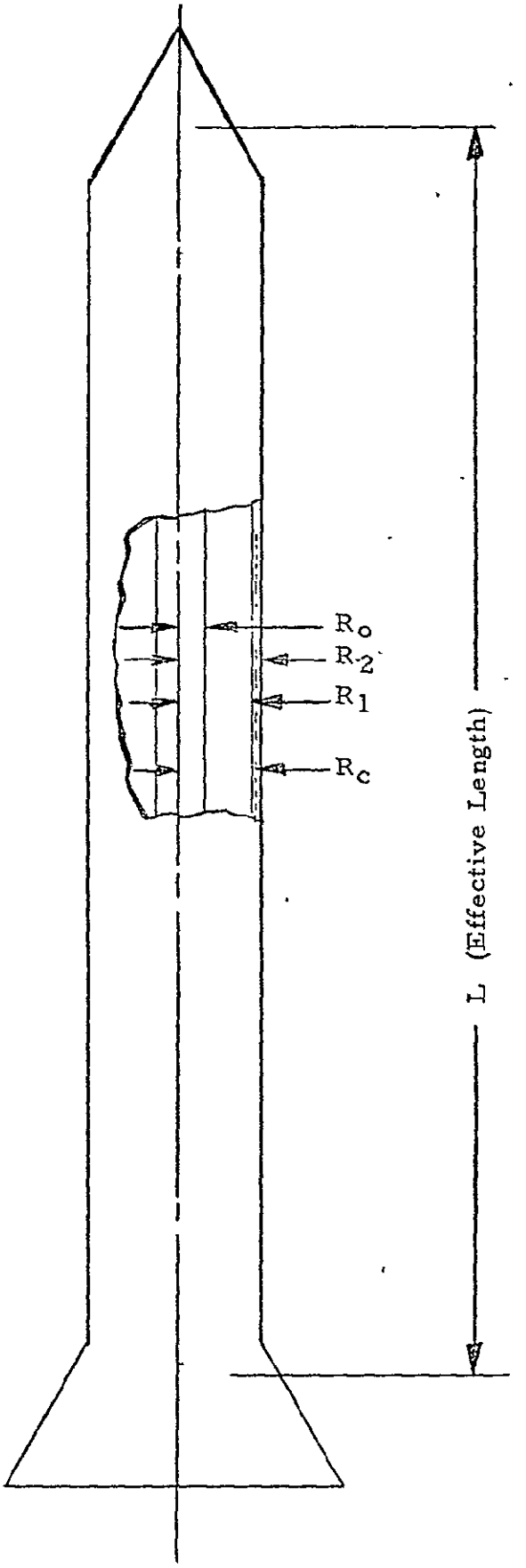

Figure 3-3. Geometric Solid Rocket Parameters Effecting the Free-Free Bending Mode

Using the following values gives

$R_c = 77.74$ in.

$R_1 = 77.474$ in.

$R_o = 24.73$ in.

$h = 0.526$ in.

$A_c = 2\pi R_c h = 257 \text{ in}^2$

$A_p = \pi (R_1^2 - R_o^2) = 16,940 \text{ in}^2$

$I_c = \pi R_c^3 h = 7.76 \times 10^5 \text{ in}^4$

$I_p = \pi/4 (R_1^4 - R_o^4) = 2.8 \times 10^7 \text{ in}^4$

$\gamma_c = .28\#/\text{in}^3$

$\gamma_p = .064\#/\text{in}^3$

$(\gamma I)_T = \gamma_c I_c + \gamma_p I_p = 2.01 \times 10^6 \#\text{-in}$

$(\gamma A)_T = \gamma_c A_c + \gamma_p A_p = 1.157 \times 10^3 \text{ lb/in}$

$G_c = E_c/3 = 9.33 \times 10^6 \text{ in}^4$

$f = 5.5$ Hz

where $f = \omega/2$

3.3 Longitudinal Free-Free Rod Modes

These modes are the longitudinal resonance of the case wherein the mass of the propellant must be considered, but the stiffness of the propellant is negligible compared to the stiffness of the case. These modes would exist only during transportation and/or handling operations of the SRB because in the assembled Space Shuttle configuration the case is restrained at its attachment points to the External Tank. This mode was determined from the following equation as obtained from Reference 18.

$$f_n = \frac{n}{2L} \sqrt{\frac{A_c E_g}{A_c \gamma_c + A_p \gamma_p}}$$

Using the following values representative of the SRB give

$n = 1$ for first mode

$A_c = 222.3 \text{ in}^2$

$A_p = 14357.9 \text{ in}^2$

$P_c = .28\#/\text{in}^3$

$P_p = .064\#/\text{in}^3$

$E = 28 \times 10^6\#/\text{in}^2$

$g = 386 \text{ in/sec}^2$

$L = 1200 \text{ in}$

$f_1 = 20.6 \text{ Hz}$

3.4 Case Radial Hoop Mode (Extensional)

This mode is characterized by a cylinder whose radius is varying as some function of time. Reference 18 indicates that the frequency of this mode can be obtained from the equation of motion for a differential element, d θ, of a solid motor cross-section which is

$$d\bar{m}\,\ddot{u} + k\,u = f(p)$$

The solution to this equation is given in Reference 18 as follows:

$$f = \frac{1}{2}\pi\sqrt{\frac{E_c\, h\, g}{(1 - \frac{\nu_c}{2})R_1\left[\frac{(R_1^2 - R_o^2)\,\gamma_p\,\bar{M}/M}{2g} + R_c h\,\gamma_c\right]}}$$

Using the following values representative of the SRB gives

$E_c = 28 \times 10^6$ psi

$h = 0.612$ in

$g = 386$ in/sec^2

$\nu_c = .3$

$R_0 = 20$ in

$R_1 = 70,388$ in

$R_c = 70.69$ in

$\gamma_p = .064$ #/in^3

$\gamma_c = .28$ #/in^3

$\bar{m}/m = 1800$

$f = 63.6$ Hz

3.5 Lobar Modes (Inextensional)

These modes are characterized by displacements developed in the propellant when the motor case undergoes arbitrary inextensional circumferential deformations. Strain variations within the propellant occur only within the lateral plane. The mode shapes of the case and propellant for the first 3 modes are as shown in Figure 3-2. Methods for calculating the lobar frequencies are described in Reference 14. From "Frequency vs. Internal Diameter to External Diameter Ratios" plots in reference document the fundamental lobar mode for the SRB is expected to be approximately 7 Hertz.

3.6 Thickness Shear Modes

These modes are characterized by displacements developed in the propellant in the longitudinal direction. The mode shapes for the first 3 modes for the axisymmetric and antisymmetric modes are shown for a slice of a solid rocket motor in Figure 3-3. The resonant frequency for the longitudinal thickness shear modes are claculated below by equations derived by Baltrukonis and Gottenburg (Reference 6) for an infinitely long hollow cylinder clamped at the outer diameter and free at the inner diameter. The infinitely long cylinder condition is one where only longitudinal displacements occur (i.e., no radial or circumferential displacements). It is shown in Section 4 that the infinitely long cylinder condition is approached by even segment lengths of the SRB.

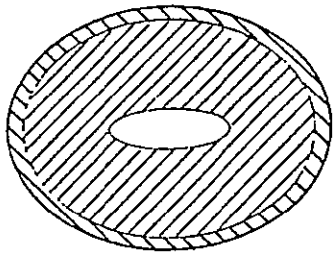

1ST MODE

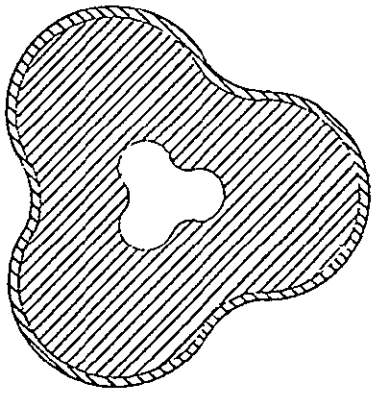

2ND MODE

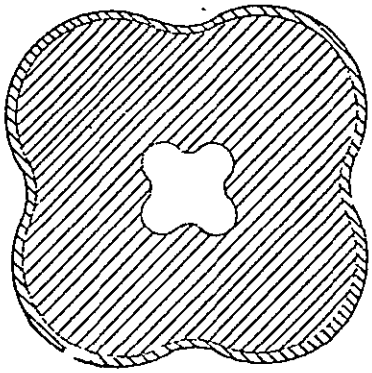

3RD MODE

Figure 3-2. Lobar Mode Shapes

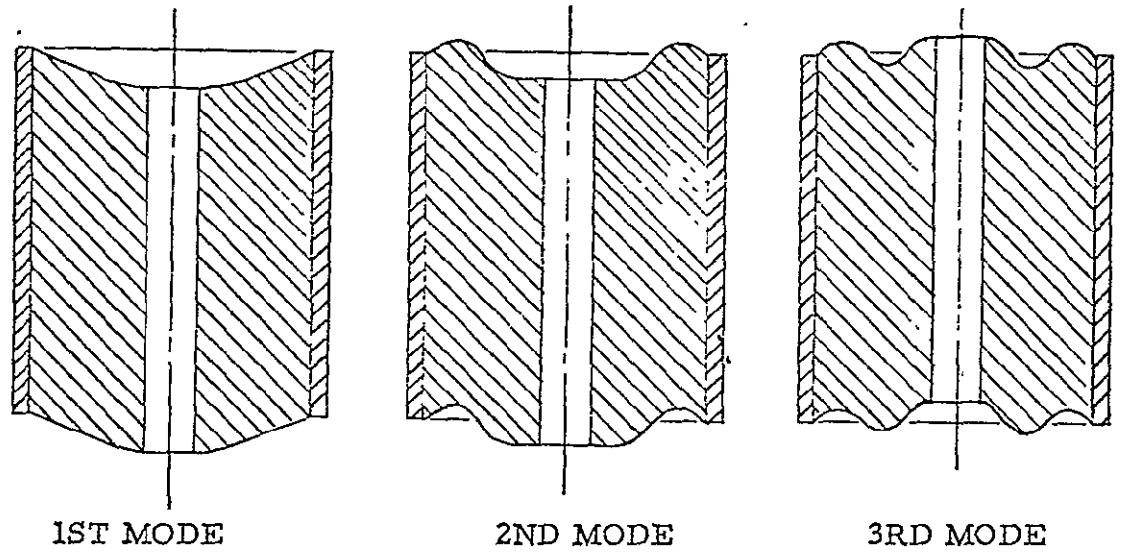

Axisymetric Modes

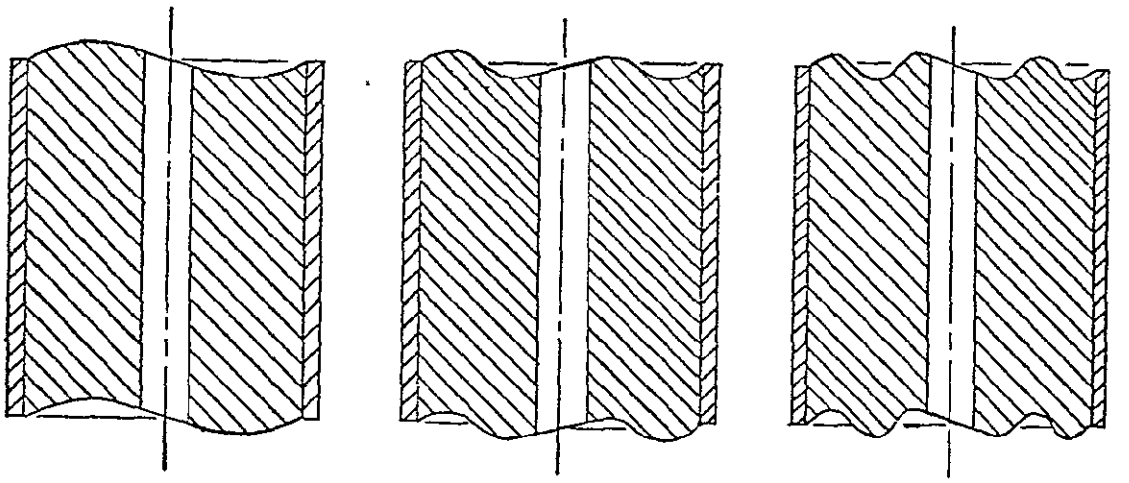

Antisymetric Modes

Figure 3-3. Longitudinal Thickness Shear Mode Shapes

Axisymmetric modes

$$f_m = 1/2\pi \ \Omega_m \sqrt{G/\rho R_1^2}$$

Using the following values representative of the SRB give

$G = 900\, f^{0.145}$ (from Section 2)

$\rho = .064/g$

Ω_1, $-\Omega_2$, and $\Omega_3 = 2.74$, 6.85 and 11.18 (from Reference 6) for $R_o/R_1 = 20/70 = .2857$

f_1, f_2 and $f_3 = 17.9$, 48.1 and 81.5 Hz

Antisymmetric modes

$$f_{1\,m} = 1/2\pi\, \Omega_m \sqrt{G/\rho R_1^2}$$

Using the same values for G, P and R_2 as above and the following, gives

Ω_1, Ω_2 and $\Omega_3 = 3.48$, 7.15 and 11.2 (from Reference 6) for $R_o/R_1 = 20/70 = .2857$

f_{11}, f_{12} and $f_{13} = 23.2$, 50.3 and 81.6 Hz

3.7 Motor Chamber Acoustic Modes

Self-generating vibration environments depend on the motor chamber acoustic modes. Most of the modes will occur at frequencies too high to excite structural vibration modes of a solid rocket except the longitudinal chamber fundamental mode. Solid rocket manufactures have computer programs to accurately compute acoustic modes for even the most complex chamber geometries. Some of the techniques are described in References 29 and 49.

The fundamental chamber mode for the SRB can be calculated by treating the chamber as a cylinder (Reference 18). The acoustic frequencies can then be calculated from the following equation:

$$f_{m,\ n,\ q} = \frac{c}{2}\sqrt{\left(\frac{q}{L}\right)^2 + \frac{(\alpha\ m\ n)^2}{R_o}}$$

Using the following values gives the frequencies listed in Table 3-3 below.

L = 42,275 in/sec

L = 1190 to 1400 (effective length including effects of radial slots in propellant and segment joints)

R_o = 20 in

α_{mn} = values were taken from Reference 18 and are listed in Table 3-2 below.

m \ n	0	1	2
0	0	1.2197	2.2331
1	0.5861	1.697	2.714
2	0.9722	2.1346	3.1734

Table 3-2. Characteristic Value (α_{mn}) for Transverse Waves

Mode ($f_{m,n}$)	Frequency (Hz)	Wave Motion
$f_{0,0,1}$	15-18	Pure longitudinal (closed-closed)
$f_{1,0,0}$	620	Pure tangential (fundamental)
$f_{2,0,0}$	1027	Pure tangential (second harmonic)
$f_{0,1,0}$	1289	Pure radial (fundamental)
$f_{0,2,0}$	2360	Pure radial (second)
$f_{1,1,0}$	1794	Coupled transverse
$f_{2,1,0}$	2256	Coupled transverse
$f_{1,2,0}$	2868	Coupled transverse
$f_{2,2,0}$	3354	Coupled transverse

Table 3-3. SRB Motor Chamber Acoustic Resonant Frequencies

The longitudinal (closed-closed) acoustic mode, $f_{0,0,1}$, consists of an oscillating pressure wave within the motor chamber. The magnitude of the pressure at the closed ends of motor chamber varies sinusoidally. This pressure oscillation will introduce oscillating extensions in the motor case which can be expected to excite the longitudinal thickness shear mode (using G = 1365 for high strains. High response levels are not expected to occur however because (1) the propellant is a heavily damped material and (2) the longitudinal shear mode is excited by the case which is at a node point. A very high driving point mechanical impedance is therefore required to vibrate the case.

3.8 Importance of Longitudinal Thickness Shear Mode

The main effort of this study task was directed towards evaluating the fundamental longitudinal thickness shear mode. There are several reasons for this. First the fundamental axisymmetric thickness shear mode can be excited by the motor chamber longitudinal acoustic mode (see paragraphs 3.6 and 3.7). A thorough analysis of this mode is therefore considered necessary. Second, at the fundamental shear frequency and its overtones there exists a strong possibility of coupling with SRB flexural and other total vehicle (Shuttle) modes. Third, the requirements for a vibration test of the longitudinal thickness shear mode led to further study to determine the feasibility of a segment test and an optimization of the size of the test segment.

4.0 LONGITUDINAL THICKNESS SHEAR VIBRATION MODE

4.1 Introduction

This section will be devoted to the longitudinal thickness shear vibration mode of the SRB. First the eigenvalues, eigenvectors, and strain distribution for a hollow cylinder, which is traction-free at the inner surface, will be determined for real values of the dynamic shear modulus. This work will then be used to show the effects on the eigenvalues of the dynamic shear modulus for high and low strain values. Next, the eigenvalue analysis for complex moduli will be compared with eigenvalue analysis for real moduli. This analysis will be supported with the comparison of the results of the real eigenvalue analysis and complex eigenvalue analysis and complex eigenvalue analysis of Nastran. The section will be completed with the discussion of the effects of length and diameter of a test segment.

4.2 Hollow Circular Bar Clamped Along Its Outer Surface

An exact solution of the three-dimensional elasticity equations of motion in cylindrical coordinates will be obtained for the axisymmetric thickness-shear vibration mode of a hollow circular cylinder which is traction free at the inner surface and clamped along the outer surface. The solution will consist of the eigenvalues, the eigenvectors, and the strain distribution. The solution of this problem was presented by J. H. Baltrukonis and W. G. Gottenberg in "Thickness Shear Vibrations of Circular Bars" (Reference 6).

For the axisymmetric thickness-shear mode, the cylinder is assumed to be infinitely long, since only then is pure thickness-shear vibration possible, and displacements occur only in the longitudinal z direction. Therefore, we can take the components of displacement to be

$$u_r = u_\theta = 0 \qquad (1a)$$

$$u_z = u_z(r, t) \qquad (1b)$$

The three-dimensional elasticity equations of motion in cylindrical coordinates are

$$\rho \frac{\partial^2 u_r}{\partial t^2} = (\lambda + 2\mu) \frac{\partial \Delta}{\partial r} - \frac{2\mu}{r} \frac{\partial \varpi_z}{\partial \theta} + 2\mu \frac{\partial \varpi_\theta}{\partial z}, \tag{2a}$$

$$\rho \frac{\partial^2 u_\theta}{\partial t^2} = (\lambda + 2\mu) \frac{1}{r} \frac{\partial \Delta}{\partial \theta} - 2\mu \frac{\partial \varpi_r}{\partial z} + 2\mu \frac{\partial \varpi_z}{\partial r}, \tag{2b}$$

$$\rho \frac{\partial^2 u_z}{\partial t^2} = (\lambda + 2\mu) \frac{\partial \Delta}{\partial z} - \frac{2\mu}{r} \frac{\partial}{\partial r}(r\varpi_\theta) + \frac{2\mu}{r} \frac{\partial \varpi_r}{\partial \theta}, \tag{2c}$$

in which

$$\Delta = \frac{1}{r} \frac{\partial (r u_r)}{\partial r} + \frac{1}{r} \frac{\partial u_\theta}{\partial \theta} + \frac{\partial u_z}{\partial z}, \tag{2d}$$

and

$$2\varpi_r = \frac{1}{r} \frac{\partial u_z}{\partial \theta} - \frac{\partial u_\theta}{\partial z}, \quad 2\varpi_\theta = \frac{\partial u_r}{\partial z} - \frac{\partial u_z}{\partial r}, \quad 2\varpi_z = \frac{1}{r}\left(\frac{\partial (r u_\theta)}{\partial r} - \frac{\partial u_r}{\partial \theta}\right) \tag{2e}$$

In view of Equation (1) these equations of motion reduce to the following single equation:

$$\frac{\partial^2 u_z}{\partial r^2} + \frac{1}{r} \frac{\partial u_z}{\partial r} = \frac{\rho}{G} \frac{\partial^2 u_z}{\partial t^2} \tag{3}$$

If we now take

$$u_z = W(r)\, e^{i\omega t} \tag{4}$$

where W(r) is a function of r only, Equation (3) becomes

$$W'' + \frac{W'}{r} + \frac{\rho \omega^2}{G} W = 0 \tag{5}$$

where primes denote differentiation with respect to r. This differential equation is the zero-order Bessel's equation whose solution is

$$W(r) = C_1 J_o\left(r\sqrt{\frac{\rho \omega^2}{G}}\right) + C_2 Y_o\left(r\sqrt{\frac{\rho \omega^2}{G}}\right) \tag{6}$$

where C_1 and C_2 are arbitrary constants and J_o and Y_o are the zero-order Bessel functions of the first and second kinds, respectively.

The strain-displacement relations in cylindrical coordinates are given by:

$$\epsilon_r = \frac{\partial u_r}{\partial r} \tag{7a}$$

$$\epsilon_\theta = \frac{1}{r} \frac{\partial u_\theta}{\partial \theta} + \frac{u_r}{r} \tag{7b}$$

$$\epsilon_z = \frac{\partial u_z}{\partial z} \tag{7c}$$

$$\gamma_{r\theta} = \frac{1}{r}\frac{\partial u_r}{\partial \theta} - \frac{u_\theta}{r} + \frac{\partial u_\theta}{\partial r} \tag{7d}$$

$$\gamma_{rz} = \frac{\partial u_r}{\partial z} + \frac{\partial u_z}{\partial r} \tag{7e}$$

$$\gamma_{r\theta} = \frac{\partial u_\theta}{\partial z} + \frac{1}{r}\frac{\partial u_z}{\partial \theta} \tag{7f}$$

In view of Equations (1), Equations (7) reduce to

$$\epsilon_r = \epsilon_\theta = \epsilon_z = \gamma_{r\theta} = \gamma_{\theta z} = 0 \tag{8a}$$

$$\gamma_{rz} = \frac{\partial u_z}{\partial r} \tag{8b}$$

so that we have only one nonzero component of strain.

The stress-strain relations in cylindrical coordinates are given by

$$\sigma_r = 2G\left(\epsilon_r + \frac{\nu}{1-2\nu}\Delta\right) \tag{9a}$$

$$\sigma_\theta = 2G\left(\epsilon_\theta + \frac{\nu}{1-2\nu}\Delta\right) \tag{9b}$$

$$\sigma_z = 2G\left(\epsilon_z + \frac{\nu}{1-2\nu}\Delta\right) \tag{9c}$$

$$\tau_{r\theta}, \tau_{rz}, \tau_{\theta z} = G(\gamma_{r\theta}, \gamma_{rz}, \gamma_{\theta z}) \tag{9d}$$

In view of Equations (8), Equations (9) become

$$\sigma_r = \sigma_\theta = \sigma_z = \tau_{r\theta} = \tau_{\theta z} = 0 \tag{10a}$$

$$\tau_{rz} = G\frac{\partial u_z}{\partial r} \tag{10b}$$

and we see that we have only a single nonzero stress component. By Equations (4) and (6), Equation (10b) becomes

$$\tau_{rz} = -G\sqrt{\frac{\rho\omega^2}{G}}\left[C_1 J_1\left(r\sqrt{\frac{\rho\omega^2}{G}}\right) + C_2 Y_1\left(r\sqrt{\frac{\rho\omega^2}{G}}\right)\right] \tag{11}$$

The displacement function, Equation (6), and the strain function, Equation 11, were developed for arbitrary boundary conditions. The substitution of the appropriate boundary conditions will give the solution of the axisymmetric thickness-shear mode of a hollow cylinder, traction free at the inner surface and clamped along the outer surface. These boundary conditions are

$$u_z\Big|_{r=b} = 0 \tag{12a}$$

$$\tau_{rz}\Big|_{r=a} = 0 . \tag{12b}$$

Substitution of Equation (12a) into Equation (4) and Equation (6) gives

$$0 = C_1 J_o \left(b\sqrt{\frac{\rho\omega^2}{G}}\right) + C_2 Y_o \left(b\sqrt{\frac{\rho\omega^2}{G}}\right) \tag{13a}$$

Substitution of Equation (12b) into Equation (11) gives

$$0 = C_1 J_1 \left(a\sqrt{\frac{\rho\omega^2}{G}}\right) + C_2 Y_1 \left(a\sqrt{\frac{\rho\omega^2}{G}}\right) \tag{13b}$$

This system of two homogeneous, linear algebraic equations in the unknown constants C_1 and C_2 can have a solution only if the determinant of the coefficients of the unknown vanishes. Therefore, the frequency equation can be written as

$$J_o \left(b\sqrt{\frac{\rho\omega^2}{G}}\right) Y_1 \left(a\sqrt{\frac{\rho\omega^2}{G}}\right) - J_1 \left(a\sqrt{\frac{\rho\omega^2}{G}}\right) Y_o \left(b\sqrt{\frac{\rho\omega^2}{G}}\right) = 0 \tag{14a}$$

or $$J_o (\Omega_m) Y_1 \left(\Omega_m \frac{a}{b}\right) - J_1 \left(\Omega_m \frac{a}{b}\right) Y_o (\Omega_m) = 0, \tag{14b}$$

where Ω_m is a circular frequency coefficient given by

$$\Omega_m = b\sqrt{\frac{\rho\omega_m^2}{G}} \tag{15}$$

the frequency number m being appended to identify the zero of the frequency Equation (14b) e.g., Ω_1 is the smallest value of Ω for which Equation (14b) is zero, Ω_2 is the next higher, etc. The zero of Equation (14b) are tabulated in Table 4-1 for several inner radius to outer radius (a/b) ratios.

a/b \ m	1	2	3
0.01	2.405	5.522	8.660
0.1	2.448	5.726	9.096
0.3	2.786	6.994	11.39
0.333	2.879	7.312	11.93
0.5	3.588	9.604	15.82
0.667	5.104	14.28	23.65
0.7	5.619	15.85	26.26
0.833	9.776	28.40	47.20
0.9	16.04	47.24	78.61
0.95	31.74	94.36	157.1
0.99	159.0	476.1	793.3

Table 4-1. Circular Frequency Coefficients

The eigenvalues can be found by using Table 4-1 and the following

$$\omega_m = \Omega_m \sqrt{\frac{G}{\rho b^2}} \quad . \tag{16}$$

The eigenvectors can be found by combining Equation (4), Equation (6), Equation (13a), and Equation (15), and by letting

$$S = \frac{C_1 e^{i\omega t}}{b} \quad . \tag{17}$$

The eigenvectors are given by

$$\frac{u_z}{b} = S \left[J_o \left(\Omega_m \frac{r}{b} \right) - \frac{J_o(\Omega_m)}{Y_o(\Omega_m)} Y_o \left(\Omega_m \frac{r}{b} \right) \right] \tag{18}$$

The strain distribution can be found by combining Equation (11) and Equation (13a). The strain distribution is given by

$$\tau_{rz} = -SG\Omega_m \left[J_1 \left(\frac{r}{b} \Omega_m \right) - \frac{J_o(\Omega_m)}{Y_o(\Omega_m)} Y_1 \left(\frac{r}{B} \Omega_m \right) \right] \tag{19}$$

Equation (16) and Equation (18) will be used in subsequent paragraphs to find the eigenvalues and eigenvectors for different values of shear moduli. They will also be used for comparison in the test segment length investigation using Nastran.

4.3 Effects of Properties on Eigenvalues

In this section the effects of eigenvalues will be discussed. The discussion will begin with the calculation of eigenvalues for infinite length cylinder for high and low strains using the eigenvalue equations derived in section 4.2 and the shear moduli of section 2.3.2. Then the effects of complex moduli on the eigenvalue will be shown. The disucssion will close with the presentation of Nastran results to show the effects of high vs. low strains and real vs. complex moduli.

4.3.1 Eigenvalues for High and Low Strains

The eigenvalues for an infinitely long hollow cylinder traction free at the inner surface and clamped at the outer surface were found in section 2.3.2 to be

$$\omega_m = \Omega_m \sqrt{\frac{G}{\rho b}}, \qquad (1)$$

where Ω_m is tablulated in Table 4-1 for various a/b ratios. An outer radius of 70 inches and an inner radius of 20 inches will be used. Therefore a/b is 0.286, and Ω_1 is found to be 2.74 by interpolating in Table 4-1. In section 2.3.2 the shear storage modulus for high and low strains were given as a function of frequency, therefore by substitution into equation (1) we can find the real eigenvalues for high and low strains.

4.3.1.1 Low Strains

The shear modulus for low strains was found to be

$$G' = 2800\, f^{0.22}, \qquad (2)$$

therefore the eigenvalue for low strain is

$$\omega_1 = 2.74 \sqrt{\frac{2800\ f_1^{0.22} \times 386}{0.064 \times 70^2}} \qquad (3)$$

Since $$2\pi f = \omega, \qquad (4)$$

$$f_1 = \frac{2.74}{2\pi} \sqrt{3446\ f_1^{0.22}}, \qquad (5)$$

or $$f_1 = 25.6\, f_1^{0.11} \qquad (6)$$

Solving equation (6)

$$f_1 = 38.1 \text{ hz} . \tag{7}$$

This corresponds to a shear modulus of

$$G' = 6244 \text{ psi} \tag{8}$$

4.3.1.2 High Strains

The shear modulus for high strains was found to be

$$G' = 900 f^{0.145} , \tag{9}$$

therefore the eigenvalue for high strains is

$$\omega_1 = 2.74 \sqrt{\frac{900 f_1^{0.145} \times 386}{0.064 \times 70^2}} \tag{10}$$

$$\text{or} \quad f_1 = \frac{274}{2\pi} \sqrt{1108 f_1^{0.145}} \tag{11}$$

$$\text{Therefore} \quad f_1 = 14.5 f^{0.0725} . \tag{12}$$

Solving equation (12)

$$f_1 = 17.9 \text{ hz} \tag{13}$$

This corresponds to a shear modulus of

$$G' = 1365 \text{ psi} . \tag{14}$$

4.3.1.3 Normalized Eigenvectors

The eigenvectors for an infintely long hollow cylinder free at the inner surface and clamped at the outer surface are given by equation (18) in section 4.2. This equation will now be solved for a cylinder with an inner radius of 20 inches and an outer radius of 70 inches. The circular frequency coefficient, Ω_1, is therefore 2.74. The eigenvectors are given by

$$u_z = 70S \left[J_o (0.039 r) - \frac{J_o' (2.74)}{Y_o (2.74)} Y_o (0.039r) \right] \tag{15}$$

Equation (15) is normalized and plotted in Figure 4-1. These eigenvectors will be used for comparison of the computer results.

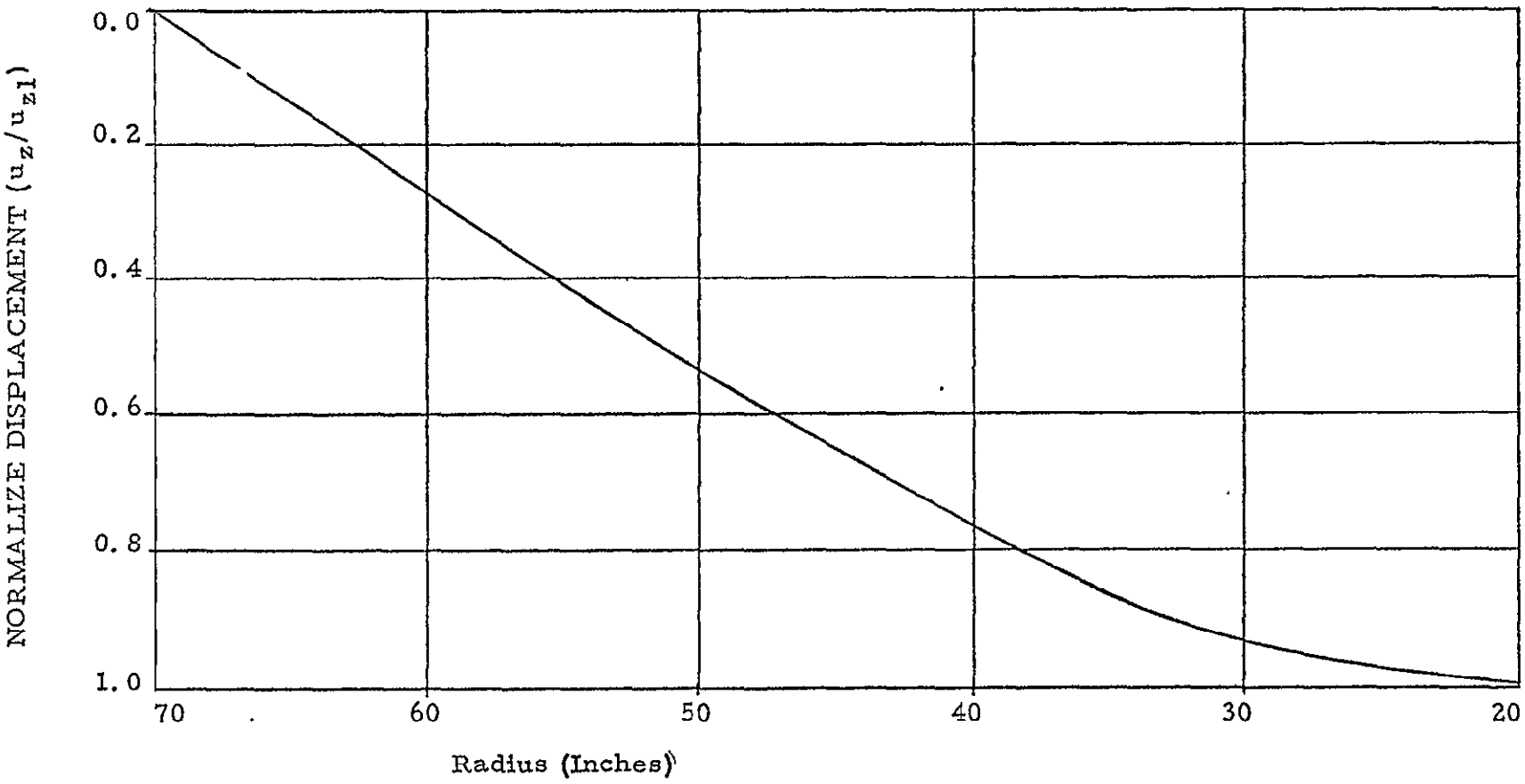

Figure 4-1. Theoretical Infinitely Long Cylinder

4.3.2 Eigenvalue Analysis

In this section a comparison will be made between real eigenvalue analysis and complex eigenvalue analysis for a multi-degree-of-freedom using matrix notation. A complex spring stiffness will be used for damping in the complex eigenvalue analysis.

4.3.2.1 Real Eigenvalue Analysis

The differential equation for an undamped multi-degree-of-freedom system using matrix notation is

$$[M]\left\{\ddot{X}\right\} + [K]\left\{X\right\} = 0. \tag{1}$$

assuming that

$$\left\{X\right\} = \left\{A\right\} e^{pt}, \tag{2}$$

Equation (1) can be written as

$$p^2 [M] + [K] = 0. \tag{3}$$

Therefore the eigenvalue is

$$p = i\sqrt{\frac{[K]}{[M]}}, \tag{4}$$

and the motion is harmonic with a frequency of $\sqrt{[K]/[M]}$ radians per second.

4.3.2.2 Complex Eigenvalue Analysis

The differential equation for a structurally damped multi-degree-of-freedom system using matrix notation is

$$[M]\left\{\ddot{X}\right\} + \left[K' + i\,K''\right]\left\{X\right\} = 0. \tag{5}$$

Assuming that

$$\left\{X\right\} = \left\{A\right\} e^{st}, \tag{6}$$

Equation (5) can be written as

$$s^2 [M] + [K' + iK''] = 0. \tag{7}$$

The eigenvalue can then be written as

$$s = i\left\{\frac{[K']}{[M]} + \frac{i\,[K'']}{[M]}\right\}^{1/2} \tag{8}$$

Letting

$$g = \frac{[K'']}{[K']}\,, \tag{9}$$

Equation (8) can be written as

$$s = p\left\{1 + ig\right\}^{1/2}. \tag{10}$$

Now to take a root of a complex number we must first express it in exponent form. Therefore

$$\left\{1 + ig\right\} = \left\{1 + g^2\right\}^{1/2} e^{ie}\,, \tag{11}$$

where $\tan \theta = g.$ (12)

now $$\left\{1 + ig\right\}^{1/2} = \left\{1 + g^2\right\}^{1/4} e^{i\frac{\theta}{2}}. \tag{13}$$

The exponential form of a complex number may be expanded as

$$e^{i\frac{\theta}{2}} = \cos\frac{\theta}{2} + i\sin\frac{\theta}{2}, \tag{14}$$

which can be written as

$$e^{i\frac{\theta}{2}} = \left(\frac{1 + \cos\theta}{2}\right)^{1/2} + i\left(\frac{1-\cos\theta}{2}\right)^{1/2}. \tag{15}$$

Since

$$\cos\theta = \frac{1}{(1 + g^2)^{1/2}}\,, \tag{16}$$

Equation (15) can be reduced to

$$e^{i\frac{\theta}{2}} = \frac{\left\{(1 + g^2)^{1/2} + 1\right\}^{1/2}}{\left\{2\,(1 + g^2)^{1/2}\right\}^{1/2}} + i\,\frac{\left\{(1 + g^2)^{1/2} - 1\right\}^{1/2}}{\left\{2\,(1+g^2)^{1/2}\right\}^{1/2}} \tag{17}$$

Combining Equation (10, Equation (13), and Equation (17), the eigenvalues can be written as

$$s = \frac{p}{\sqrt{2}}\left\{\left[(1 + g^2)^{1/2} + 1\right]^{1/2} + i\left[(1 + g^2)^{1/2} - 1\right]^{1/2}\right\}. \tag{18}$$

If we take the undamped natural frequency as

$$\omega_n = \sqrt{\frac{[K]}{[M]}} , \tag{19}$$

Equation (18) can be written as

$$s = -\frac{\omega n}{2}\left\{(1+g^2)^{1/2}-1\right\}^{1/2} + i\frac{\omega n}{2}\left\{(1+g^2)^{1/2}+1\right\}^{1/2} . \tag{20}$$

Therefore the equations of motion can be written as

$$\{X\} = \{A\}\ e^{(-\alpha + i\omega)t} , \tag{21}$$

where

$$\alpha = \frac{\omega_n}{\sqrt{2}}\left\{(1+g^2)^{1/2}-1\right\}^{1/2} \tag{22}$$

and

$$\omega = \frac{\omega_n}{\sqrt{2}}\left\{(1+g^2)^{1/2}+1\right\}^{1/2} . \tag{23}$$

Therefore the motion is harmonic with a frequency of ω and decaying at the rate α. It is interesting to note that since g is a positive number

$$\left\{(1+g^2)^{1/2}+1\right\}^{1/2} > 2 , \tag{24}$$

and the harmonic frequency of a system with structural damping is greater than that of the undamped system.

4.3.3 Effect of Moduli on Nastran Results

This section will show the effects of the high versus low modulus and real versus complex modulus on the eigenvalues and eigenvectors of the Nastran results. A comparison of the eigenvalues and eigenvectors will be made with the exact solution for an infinitely low elastic cylinder from section 4.3.1. The computer model used in this comparison is 300 inches in length. A comparison of different segment lengths is made in section 4.4.1.

Table 4-2 shows the effects on the eigenvalue caused by using a real and complex shear modulus

	Low Strains	High Strains
Theoretical Solution	38.1 Hz	17.9 Hz
Real Modulus	38.2	17.9
Complex Modulus	38.8	18.0

Table 4-2. Effect of Moduli on Eigenvalue

associated with high strain and low strains. The shear moduli for the real solutions are 6244 psi for low strains and 1365 psi for high strains. The shear moduli for the complex solutions are 6244 (1+i0.384) for low strains and 1365 (1+ i 0.245) for high strains. Table 4-2 shows that there is good agreement of the eigenvalues for the theoretical solution and the normal eigenvalue analysis. The eigenvectors are compared in section 4.4.1. Table 4-2 also shows that the eigenvalues for the complex analysis are higher than those from the normal analysis. This is expected for the reasons discussed in section 4.3.2. The increase is greater for the low strains because the complex part is a higher percentage of the real part.

4.4 Effects of Size on the Thickness Shear Mode

This section will discuss the effects of the segment size on the eigenvalues, the eigenvectors, and the strain levels. The effect of segment length will be shown by using Nastran models of different lengths. The effects of varying the segment inner diameter and outer diameter will be discussed by studying the equations developed in section 4.2. To aid in the discussion, the eigenvalue problem of a solid circular cylinder clamped at the outer surface will be developed.

4.4.1 Effect of Length

Three different NASTRAN models were used to study the effects of segment length on the thickness shear mode. The models were identical in all respects except that one dimension of the elements was adjusted so that the model could have a total length of 100 inches, 150 inches, and 300 inches. The model is discussed in Appendix B. The model was run at both high and low values for the shear modulus using normal mode analysis. Table 4-3 shows the effects of varying the length on the eigenvalue. Also shown are the theoretical eigenvalues for an infinitely long cylinder which were calculated in section 4.3.1. The eigenvectors for the various length are shown in Figure 4-2. The eigenvectors for the infinite length are obtained from section 4.3.1.

LENGTH	HIGH MODULUS	LOW MODULUS
100 Inches	37.0 Hz	17.3 Hz
150	37.7	17.6
300	38.2	17.9
∞	38.1	17.9

Table 4-3. Eigenvalues Versus Length

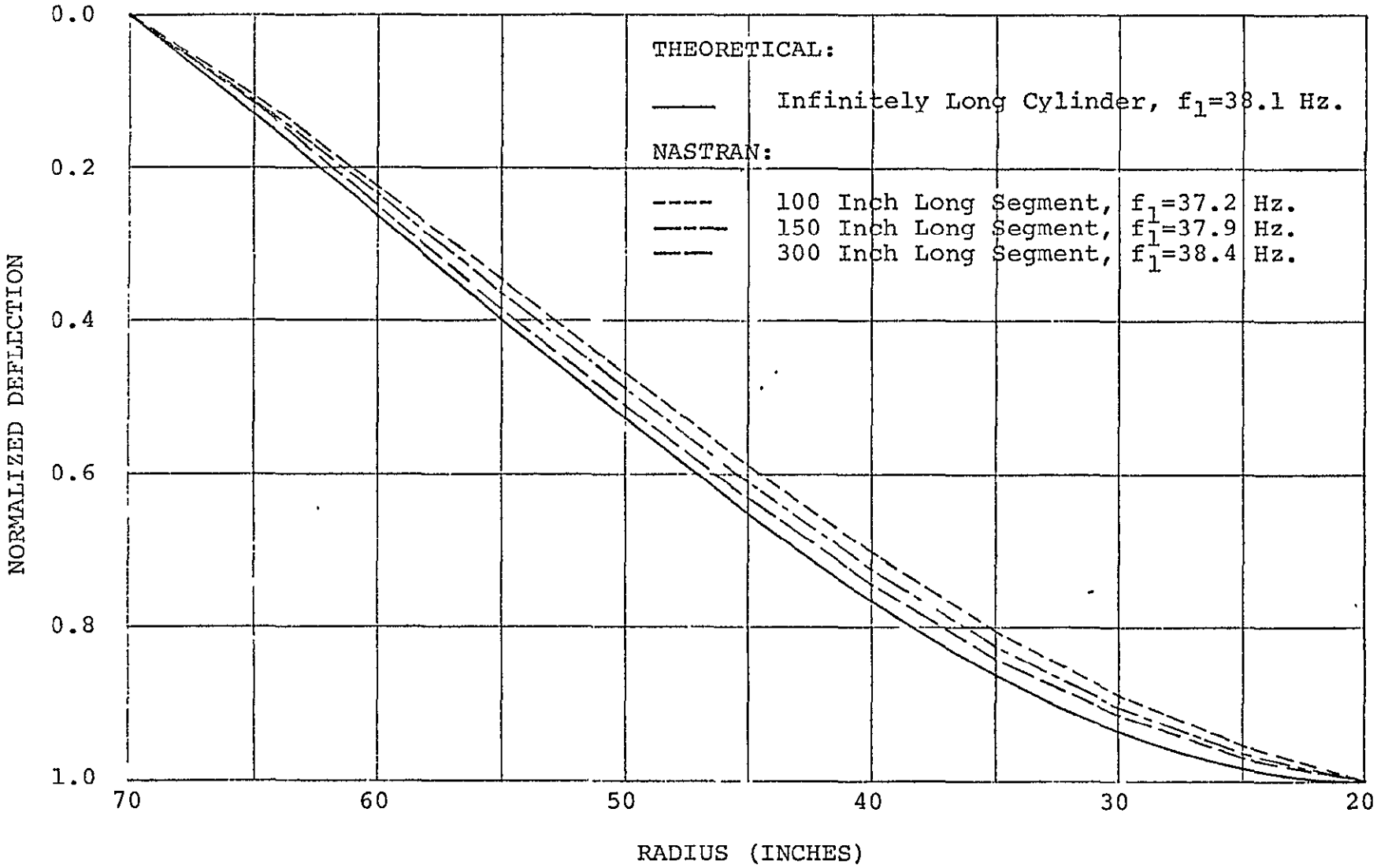

FIGURE 4-2. REAL EIGENVECTORS OF FIRST THICKNESS SHEAR MODE FOR HIGH SHEAR MODULUS

The eigenvectors shown are normalized and, therefore, are not influenced by a change in modulus.

Table 4-3 and Figure 4-2 show that the solution of the eigenvalue problem depends on the length of the segment. The solution of the problem approaches that of an infinite length as the length is increased. The length of the segment was not made greater than 300 inches due to the natural boundary conditions made during manufacturing. It assumed that a vehicle segment will be approximately 300 inches in length.

4.4.2 Solid Circular Cylinder Clamped at the Outer Surface

The eigenvalue problem for an infinitely long elastic solid circular cylinder clamped at the outer surface will be solved to aid in the discussion of varying the outer diameter of the test specimen for a scaled-down test. The solution of the problem will be identical to that in section 4.2, only the boundary condition will change. As in section 4.2, the equations of motion can be reduced and solved as

$$W(r) = C_1 J_o \left(r\sqrt{\frac{\rho\omega^2}{G}}\right) + C_2 Y_o \left(r\sqrt{\frac{\rho\omega^2}{G}}\right) \qquad (1)$$

The boundary condition for this case is

$$u_z \Big|_{r=b} = 0 \qquad (2)$$

In order to avoid infinite displacements at the axis of the bar, C_2 must equal zero and therefore

$$J_o(\Omega m) = O \qquad (3)$$

The zero values of Ωm are given in Table 4-4.

m	Ω m
1	2.405
2	5.520
3	8.654
4	11.79
5	14.93

Table 4-4. Natural Circular Frequency Coefficients for a Solid Circular Cylinder Clamped at Its Outer Surface

The deflection is given by

$$\frac{u_z}{b} = S\, J_o \left(\Omega m \frac{r}{b}\right) \qquad (4)$$

and the strain is given by

$$\tau = -sG\, \Omega m\, J_1 \left(\Omega m \frac{r}{b}\right) \qquad (5)$$

4.4.3 Effects of Size on Test Specimen

The purpose of testing a segment is to reduce the cost of testing the total vehicle or stage, but the test will only be valid as long as the parameters that are measured in the test are not affected by the size of the test specimen. In section 4.4.1 it is shown that to produce the pure thickness shear mode the test specimen must be approximately 300 inches long. The effects of scaling the diameters is a more complex problem.

Many things must be considered when determining the effects of scaling the diameters. The moduli are functions of frequency. The moduli are difficult to measure and, therefore, the frequency between the test specimen and the vehicle should not change. Since

$$\omega_m = \Omega m \sqrt{\frac{G}{\rho b^2}} \qquad (1)$$

and m is a function of a/b, as b is decreased a would also have to be decreased to keep the eigenvalue constant. The limit would be reached when a reaches zero and the cylinder becomes solid. The limit for b can be found by using section 4.4.2. Using the values for low strains and assuming that G is only a function of frequency

$$38.1 \times 2\pi = 2.405 \sqrt{\frac{6244 \times 386}{.064 \times b^2}} \qquad (2)$$

and solving, b = 62 inches. Therefore, the smallest diameter test specimen with no change in the thickness shear mode would be 124 inches if G was only function of frequency. But it is shown in Appendix A and in section 2 that the moduli are functions of frequency and strain.

In section 4.2, it was shown that the strain is a function of the outer radius, b, and the ratio of the inner radius to outer radius. The amount of strain variation can be seen by considering the term Yo (Ωm) in equation 19 of section 4.2. At certain diameter ratios this term can go to zero. When this happens the strains can become infinite. This is only in a theoretical sense, but still, a large variation in moduli and, therefore, frequency would occur. Therefore, only the full scale diameters should be used in vibration testing.

4.5 Summary

The longitudinal thickness shear mode is a function of the modulus, density, and the physical configuration. The moduli are functions of frequency, therefore the value used to calculate the thickness shear mode must correspond to the eigenvalue. The moduli are also functions of strain, therefore the value used should correspond to the strains.

Using the complex modulus causes only a slight increase in the eigenvalue. This was shown both theoretically and with NASTRAN. The increase is slight enough to disregard the complex stiffness and use only a normal mode analysis unless very accurate results are needed.

An operation SRB segment should be used as the test segment to evaluate the thickness shear mode. If, however, the segment length is considerably longer than 300 inches, considerations should be given to reduce the length to 300 inches for the purpose of total test program cost reduction. The diameter of the test segment can not be sealed because the varying strain will effect the eigenvalues.

5.0 SRB TEST RECOMMENDATIONS

5.1 Type of Testing

The type of testing discussed in this section is development testing. The primary purpose of this type of testing is to evaluate the design and/or verify the analysis. It should be distinguished from qualification testing which is primarily conducted on production hardware to certify the manufacturing processes. Development tests are considered those tests which are conducted early in the program on prototype models before static firing and flight testing is performed.

5.2 Requirements for SRB Dynamic Testing

The precedent of previous vibration testing of solid rockets such as Minuteman and Titan suggest the need for full scale and individual stage vibration testing to evaluate the various modes of vibration including modes predominantly propellant oriented as well as structural modes. Although discussions with TCC and UTC indicated no design problems were revealed by development testing, they did afford a verification of analysis.

The Space Shuttle contains an External Lox/LH_2 Tank, two Solid Rocket Boosters and the Orbiter. It is much more complex structurally than the Minuteman or Titan Vehicles. Experience with Saturn V dynamic testing has shown the deficiencies of dynamic analysis where a large complex launch vehicle is involved. Although the techniques of structural analysis have improved greatly from the development periods of the Minuteman, Titan and Saturn V Vehicles, certain assumptions and analytical modeling simplifications are still required. It is these assumptions and simplifications which must still be verified by test.

5.3 Lateral Bending and Longitudinal Structral Modes

Dynamic development testing of the Space Shuttle Vehicle provides the ultimate configuration for evaluating the SRB because the exact motion restraints of the SRB attachment hardware can be realized. All structural oriented modes such as lateral bending and longitudinal modes can be ideally evaluated in the total Space Shuttle Vehicle configuration. Separate

Separate dynamic testing of the SRB for evaluating lateral bending and longitudinal modes with reasonable accuracies would require elaborate and costly simulation of the External Tank and Orbiter interfaces. These interfaces would include local stiffness of attachment hardware and mass property simulation of the External Tank and Orbiter. It is doubtful that the cost of implementing a separate SRB test would be attractive if development costs of interface hardware were considered.

Because of the above arguments, it is recommended that the SRB lateral bending and longitudinal structural modes be evaluated by a dynamic test with the SRB in the complete Space Shuttle configuration.

5.4 Propellant Modes

Propellant modes as discussed in Section 3 are the Lobar and Longitudinal Thickness Shear Modes.

The requirement to verify the analysis of propellant modes stems from the fact that the shear and elastic moduli are complex quantities which vary with strain, frequency, pressure and temperature. Solution for the propellant modes can, therefore, vary considerably based on the shear moduli data used in the analytical model.

Propellant modes are not dependent on the external motion restraints of the SRB. Separate full scale SRB stage testing could therefore be conducted to evaluate these modes. Also since it is considered necessary to evaluate the propellant modes with active propellant, there would be ignition hazards associated with propellant mode testing. It is therefore desirable to limit the risk and test the smallest configuration.

The feasibility of evaluating propellant modes with (1) a segment of the SRB and (2) a reduced scale segment were evaluated during this study. The results of the evaluation, which are summarized in section 4.4.1 and 4.4.3, show that a segment test would be a satisfactory test specimen, but a reduced scale segment would be unsatisfactory. Furthermore the length of the test segment has been established at approximately 300 inches. Based upon the above arguments, it is recommended that the Longitudinal Thickness Shear Mode analysis be verified by a SRB segment test.

5.5 Motor Chamber Acoustic Modes

Motor chamber acoustic modes are a source of self-generated vibration. Only the Fundamental Closed-Closed Longitudinal mode is low enough in frequency to excite structural modes of the SRB. Analytical techniques are considered adequate to accurately determine this mode. No development testing is therefore recommended.

5.6 Material Sample Testing

Reference 9 has shown that the elastic modulus of elastomers can vary drastically as the amount of filler material is changed. The properties

of the SRB propellant will therefore most likely have to be completely evaluated after formulation with regards to the amount of solids in the propellant is specified. Furthermore, the data available from literature and from TCC and UTC is not adequate to show the specific effects of temperature, pressure, frequency and strain level on PBAN.

In order to have the necessary data to accurately predict propellant modes, it is recommended the sample testing be performed early in the development program so that "Dynamic Shear Modulus vs. Frequency" plots can be obtained in the range of 5 to 50 Hertz at several strain levels from the lowest to the highest strains expected. It is recommended that the effects of temperature be evaluated at 30, 70 and 100 ^{o}F, and the effects of pressure be evaluated at barometric pressure and 1000 psia.

There are many test methods that can be used to evaluate dynamic shear modulus. The methods described in Reference 10 are used in the propellant industry and will probably give the best results.

APPENDIX A

DYNAMIC PROPERTIES OF VISCOELASTIC MATERIALS

SYMBOLS

E = Elastic Modulus

G = Shear Modulus

ν = Poisson's Ratio

K = Bulk Modulus

F = Force

σ = Stress

ε = Strain

η = Viscosity Coefficient

τ = Relation Time

E_r = Relaxation Modulus

E' = Elastic Storage Modulus

E'' = Elastic Loss Modulus

δ = Loss Tangent

$\zeta = \frac{C}{CC}$ = Damping Ratio

H = Distribution of Relaxation Times

T = Temperature (Absolute)

d = Density

A_T = Temperature Shift Factor

G' = Shear Storage Modulus

G'' = Shear Loss Modulus

A = Magnitude of Harmonic Function

ω = Frequency

t = Time

E^* = Complex Elastic Modulus Magnitude

ε_d = Dashpot Strain

ε_s = Spring Strain

^oK = Degrees Kelvin

APPENDIX A

Dynamic Properties of Viscoelastic Materials

1.0 INTRODUCTION

The physical properties of viscoelastic materials required for dynamic analysis will be defined and characterized in this appendix. These properties are elastic modulus, shear modulus, Poisson's ratio, and the damping ratio. Only three of the four parameters are independent, since three of the parameters are related by

$$E = 2(1 + \nu)G. \qquad (1)$$

The significance of these properties will be discussed as they relate to viscoelastic materials.

2.0 POISSON'S RATIO

Poisson's ratio is related to the bulk modulus and shear modulus by (Reference 19)

$$\nu = \frac{3K-2G}{6K+2G} \qquad (2)$$

which can be reduced to

$$\nu = \frac{3 - 2\frac{G}{K}}{6+2\frac{G}{K}} \qquad (3)$$

It is customary to assume that viscoelastic materials are incompressible; therefore the bulk modulus is infinite ($K = \infty$) and Poisson's ratio is one-half ($\nu = 0.5$). Equation (1) can then be reduced to this simple relationship

$$E = 3G \qquad (4)$$

3.0 MODULI

Since the relationship between the elastic modulus and the shear modulus for viscoelastic materials is given by equation (4), only one needs to be determined. The elastic modulus will be determined because of the ease in visualization. To aid in the development of the elastic modulus for viscoelastic materials, the stress-strain relationship for elastic materials and viscous materials will be presented. They will then be expanded to show the stress-strain relationship for viscoelastic materials.

3.1 Elastic Materials

In an elastic material (metals) operating below the elastic limit, stress is directly proportional to strain. This can be modeled by a linear spring as shown in Figure A-1.

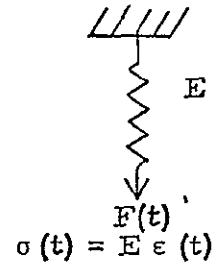

$$\sigma(t) = E\,\varepsilon(t)$$

Figure A-1. Model of Elastic Materials

It is important to note that the dependent variable $\sigma(t)$ is directly proportional to the independent variable without a phase shift during dynamic excitation. The response to step stress σ_o, is shown in Figure A-2, and the response to a step strain, ε_o, is shown in Figure A-3.

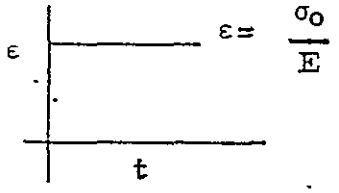

Figure A-2. Elastic Response to Step Stress

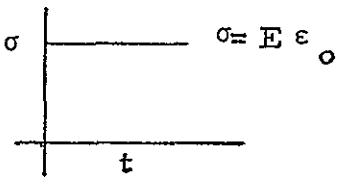

Figure A-3. Elastic Response to Step Strain

3.2 Viscous Materials

In a linear viscous material (fluids) the stress is directly proportional to the rate of strain. This can be modeled by a linear dashpot shown in Figure A-4.

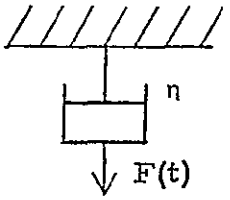

$$\sigma(t) = \eta \frac{d\varepsilon(t)}{dt}$$

Figure A-4. Model of Viscous Materials

The response of a viscous material to harmonic excitation can be found by letting

$$\varepsilon(t) = A \sin \omega t \qquad (5)$$

then $$\frac{d\varepsilon(t)}{dt} = \omega A \cos \omega t \qquad (6)$$

and $$\sigma(t) = \eta \omega A \cos \omega t \qquad (7)$$

or $$\sigma(t) = \eta \omega A \sin \left(\omega t + \frac{\pi}{2}\right) \qquad (8)$$

By observing equations (5) and (8), two important facts can be seen:

1) Stress leads strain by 90°, and

2) Stress is a function of the frequency of excitation

The response to a step stress is shown in Figure A-5. The response to a step strain is an impulse function and is not shown.

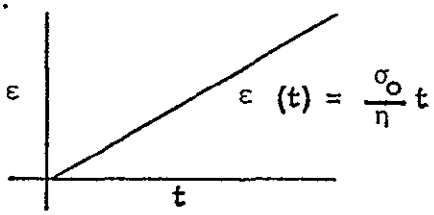

Figure A-5. Viscous Response to Step Stress

3.3 Viscoelastic Materials

As the name implies, viscoelastic materials (polymers) have some characteristics of elastic materials and some characteristics of viscous materials. Many mathematical models have been developed for viscoelastic materials. All of these models are various combinations of the spring and dashpot elements. Only the simplest model will be discussed.

Viscoelastic materials can be modeled by the spring and dashpot element in series as shown in Figure A-6. The relationship between stress and strain can be found by substituting the following identities into the equations in Figure A-6:

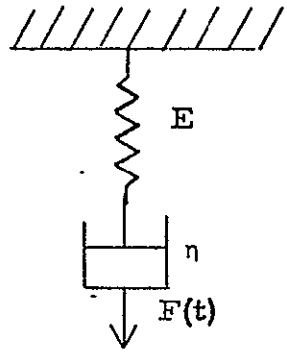

$$\varepsilon(t) = \varepsilon_s(t) + \varepsilon_d(t)$$

$$\sigma(t) = \sigma_s(t) = \sigma_d(t)$$

where s indicates spring
d indicates dashpot

Figure A-6. Simple Model of Viscoelastic Materials

$$\varepsilon_s(t) = \frac{\sigma(t)}{E} \qquad (9)$$

and $$\varepsilon_d(t) = \int \frac{\sigma(t)}{\eta}\, dt \qquad (10)$$

substituting

$$\dot{\varepsilon}(t) = \frac{\sigma(t)}{E} + \int \frac{\sigma(t)}{\eta}\, dt \qquad (11)$$

or $$\frac{d\,\varepsilon(t)}{dt} = \frac{d\,\sigma(t)}{E\,dt} + \frac{\sigma(t)}{\eta} \qquad (12)$$

By defining the relaxation time, τ, as

$$\tau = \frac{\eta}{E}, \qquad (13)$$

equation (12) can be reduced to the following form to give the relationship between stress and strain:

$$\sigma(t) = \left\{ \frac{E\,\frac{d}{dt}}{\frac{d}{dt} + \frac{1}{\tau}} \right\} \varepsilon(t) \qquad (14)$$

It can be seen that equation (14) is far more complex than that for elastic behavior. Although this math model is very simple, it can be used to obtain an understanding of the response of viscoelastic materials to various forms of excitation.

3.3.1 Viscoelastic Response to Step Functions

The response of a viscoelastic material to a step stress is commonly called creep. The strain resulting from a step stress is

$$\varepsilon(t) = \frac{\sigma_o}{E} + \int \frac{\sigma_o}{\eta}\, dt \qquad (15a)$$

or

$$\varepsilon(t) = \frac{\sigma_o}{E} + \frac{\sigma_o t}{\eta} \qquad (15b)$$

It can be seen that initially the spring elongates an amount equal to σ_o/E and then the dashpot elongates as a function of time. The response is shown in Figure A-7.

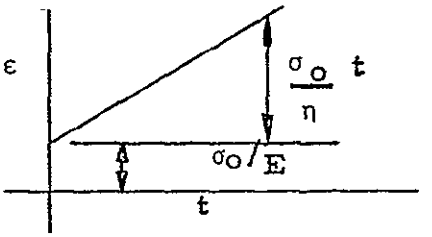

Figure A-7. Viscoelastic Response to a Step Stress

The response of a viscoelastic material to a step strain is commonly called stress relaxation. Since strain is not a function of time for a step strain

$$\frac{d\varepsilon(t)}{dt} = 0 \qquad (16)$$

therefore

$$\frac{d\sigma(t)}{dt} + \frac{\sigma(t)}{\tau} = 0 \qquad (17)$$

The solution of this differential equation is

$$\sigma(t) = \sigma_o e^{-t/\tau} \qquad (18)$$

It can be seen that the initial deformation goes into stretching the spring. Then the stretched spring exerts a force on the dashpot which elongates and allows the spring to contract reducing the force. The response is shown in Figure A-8.

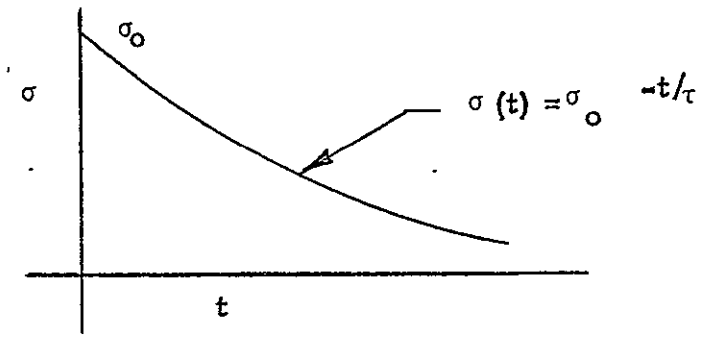

Figure A-8. Viscoelastic Response to a Step Strain

The curve in Figure A-8 is called a relaxation curve. The relaxation modulus is defined as

$$E_r(t) = \frac{\sigma}{\varepsilon} = \frac{\sigma_o}{\varepsilon} e^{-t/\tau} = E\, e^{-t/\tau} \qquad (19)$$

It is important to note that the relaxation modulus is a function of time. The relaxation modulus will be discussed again later.

3.3.2 Viscoelastic Response to Harmonic Excitation

The response of a viscoelastic material to harmonic excitation can give us important insight regarding the parameters required for modal analysis.

Letting $\varepsilon(t) = A \sin \omega t \qquad (20)$

in equation (14) yields

$$\frac{d\sigma(t)}{dt} + \frac{\sigma(t)}{\tau} = A_\omega E \cos \omega t \qquad (21)$$

The solution of this differential equation is

$$\sigma(t) = \frac{\omega EA \left(\omega \sin \omega t + \frac{1}{\tau} \cos \omega t\right)}{\frac{1}{\tau^2} + w^2} \qquad (22)$$

Since $\cos \omega t = \sin\left(\omega t + \frac{\pi}{2}\right) \qquad (23)$

$$\sigma(t) = \frac{\omega^2 EA \sin \omega t}{\frac{1}{\tau^2} + \omega^2} + \frac{\omega EA \frac{1}{\tau} \left(\sin \omega t + \frac{\pi}{2}\right)}{\frac{1}{\tau^2} + \omega^2} \qquad (24)$$

or $$\sigma(t) = \frac{\omega^2 \tau^2 EA \sin \omega t}{1 + \omega^2 \tau^2} + \frac{\omega \tau EA \left(\sin \omega t + \frac{\pi}{2}\right)}{1 + \omega^2 \tau^2} \qquad (25)$$

Since $\varepsilon(t) = A \sin \omega t$, it can be seen that there are two components in the relationship between stress and strain. One stress component is in phase with strain and the other stress component is 90° out of phase with strain. This relationship can be written as

$$\sigma(t) = (E' + iE'')(\varepsilon(t) \qquad (26)$$

or

$$\frac{\sigma(t)}{\varepsilon(t)} = E' + iE'' \qquad (27)$$

Where E' represents the in phase component and E'' represents the out of phase component. They are given for our simple model as

$$E' = \frac{\omega^2 \tau^2 E}{1 + \omega^2 \tau^2} \qquad (28)$$

and

$$E'' = \frac{\omega \tau E}{1 + \omega^2 \tau^2} \qquad (29)$$

3.3.3 Storage Modulus and Loss Modulus

E' is known as the elastic storage modulus and E'' is known as the elastic loss modulus. It is important to note that the moduli are functions of frequency. The relationships between the components are shown in Figure A-9 and Figure A-10. It should be noted that the strain lags the total stress by the phase angle δ. Since the relationship between stress and strain is a complex number, it may also be written as

$$E' + E'' = E^* e^{-\delta} \qquad (30)$$

where

$$E^* = \left\{(E')^2 + (E'')^2\right\}^{1/2} \qquad (31)$$

and

$$\delta = \tan^{-1} \frac{E''}{E'} \qquad (32)$$

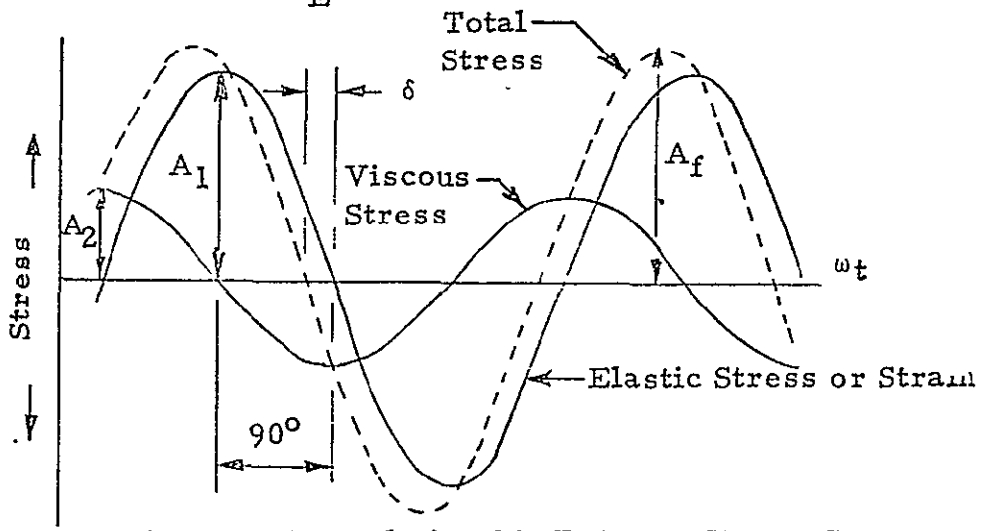

Figure A-9. Relationship Between Stress Components and Strain

3.3.4 Complex Modulus and Loss Tangent

The vector sum of the storage modulus E' and the loss modulus E'', is defined as the complex modulus E^*. This is shown in Figure A-10.

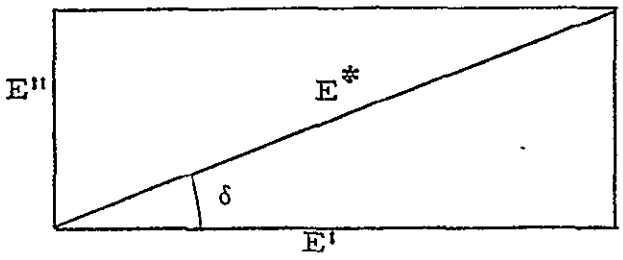

Figure A-10. Vector Representation of Complex Modulus

The parameter δ is called the loss tangent and is related to the damping ratio by

$$\frac{c}{cc} = \zeta = \frac{\tan\delta}{2} = \frac{E''}{E'} \qquad (33)$$

3.3.5 Shear Modulus

It has therefore been shown that the relationship between stress and strain for our simple model of viscoelastic materials is a complex number which is a function of frequency. Although we elected to use the elastic modulus for our development, we could have just as easily used the shear modulus. In fact, the relationship between the shear modulus and the elastic modulus given in equation (4) holds true for the complex moduli. Therefore the shear storage modulus, G', and the shear loss modulus, G'', are given by

$$E' = 3G' \qquad (34)$$

and

$$E'' = 3G'' \qquad (35)$$

3.3.6 Relaxation Modulus and Dynamic Moduli Determination

Equations (9) thru (29) were developed for a one spring-dashpot system with a relaxation time of τ. By comparing the mathematical model response in Figure A-8 with the experimental response in Figure A-11, it can be seen that the model is not representative of measured data over long time periods. A better representation can be found however, by using an infinite number of relaxation times. Therefore, the relaxation modulus can be expressed as

$$E_r(t) = E_1 e^{-t/\tau_1} + E_2 e^{-t/\tau_2} + E_3 e^{-t/\tau_3} \ldots \qquad (36)$$

or

$$E_r(t) = \lim_{n\to\infty} \sum_{i=1}^{\infty} E_i e^{-t/\tau_i} \qquad (37)$$

Equation (37) can be written in integral form as

$$E_r(t) = \int_{\tau=0} E_\infty(\tau) e^{-t/\tau} \, d\tau + E_\infty \qquad (38)$$

E_∞ is added after integration because after an infinite time the relaxation modulus ceases to decay without having reached zero. E_∞ represents the value of the relaxation modulus at that time.

Since the distribution of relaxation times is very broad, it is convenient to use logarithmic notation.

Letting $H(\ln \tau) = \tau \, E(\tau)$ (39)

$$E_r(t) = \int_{\ln\tau=-\infty}^{\infty} H(\ln \tau) e^{-t/\tau} \, d(\ln \tau) + E_\infty \qquad (40)$$

$H(\ln \tau)$ can be calculated a number of ways. A crude approximation is (Reference 17)

$$H(\ln \tau) = \frac{-d\left[Er(t)\right]}{d \ln t} \qquad (41)$$

A more accurate approximation is (Reference 17)

$$H(\ln \tau) = \frac{-d}{d \ln t}\left[Er(t)\right] + \frac{d^2\left[Er(t)\right]}{d(\ln t)^2} \qquad (42)$$

Equations (41) and (42) are evaluated under the conditions that $t = \tau$. In order to get an accurate approximate distribution of relaxation times, the experimental data should cover at least eight to fifteen decades of time. Returning to Equations (28) and (29) for dynamic moduli, they can now be expanded to give

$$E' = \int_{-\infty}^{\infty} H(\ln \tau) \frac{\omega^2 \tau^2}{1 + \omega^2 \tau^2} \, d(\ln \tau) + E_\infty \qquad (43)$$

and

$$E'' = \int_{-\infty}^{\infty} H(\ln \tau) \frac{\omega \tau}{1 + \omega^2 \tau^2} \, d(\ln \tau) \qquad (44)$$

Therefore, the complex modulus for dynamic analysis can be found by measuring the response to a step strain.

From the stress relaxation curve, the distribution of relaxation times ($H(\ln \tau)$) can be found. This distribution can then be used in the appropriate equation to determine the dynamic moduli. Computer codes have been written to aid in the mathematics. To obtain an accurate distribution of relaxation times, the relaxation curve must be known over eight to fifteen decades of time. To reduce the test time required to generate the relaxation curve and to alleviate the difficulties of obtaining data for

short times due to the inability of test equipment to apply an exact step strain, a time-temperature superposition principle may be used. This principle is explained in detail in Reference (17) and is next summarized.

The time-temperature superposition principle states that in viscoelastic materials time and temperature are equivalent to the extent that data at one temperature can be superimposed upon data taken at a different temperature merely by shifting curves. The procedures involve shifting of stress-relaxation curves taken at different temperatures along the log time axis until portions of the curves all superimpose to form one continuous curve. Before the experimental relaxation curves can be shifted to make the master curve the modulus values should be corrected for density and temperature. This correction is

$$E_r(t) \text{ reduced} = \frac{T_o d_o}{T d} E_r(t) \qquad (45)$$

where the subscript 'o' indicates a reference temperature. After this correction has been made, the curves may be plotted and then shifted to obtain a master relaxation curve. The amount of shift is given by the following equation.

$$\log A_T = \log t/t_o = \frac{-8.86\,(T-243)}{101.6 + T - 243} \qquad (46)$$

Where T is in ^{o}K, the log A_T gives the decades of time that the relaxation curves should be shifted. The principle can be illustrated by referring to Figure A-11 where the test data corrected for density and temperature is shown on the left, and the log shift factor, log A_T, is shown in the upper right. It can be seen from Figure A-11 that the log shift factor for $-40^{o}C$ is approximately +4, therefore the test data taken at $-40^{o}C$ should be shifted 4 decades to the right. The master curve in Figure A-11 does show that the test data taken at $-40^{o}C$ and 10^{o} hours has been shifted to 10^{-4} hours.

Another method (Reference 10) for determining the parameters for dynamic analysis is an emperical technique developed for determining G' and G''. The method involves vibrating a disk of the viscoelastic material and measuring its response. From this response, G' and G'' can be mathematically determined.

It was shown in Equations (43) and (44) that E' and E'' are functions of frequency. Therefore, in a dynamic analysis the modulus used has to be based on the frequency of interest. In addition to frequency, the moduli also depend on strain, temperature, and pressure. The effects of each will now be discussed.

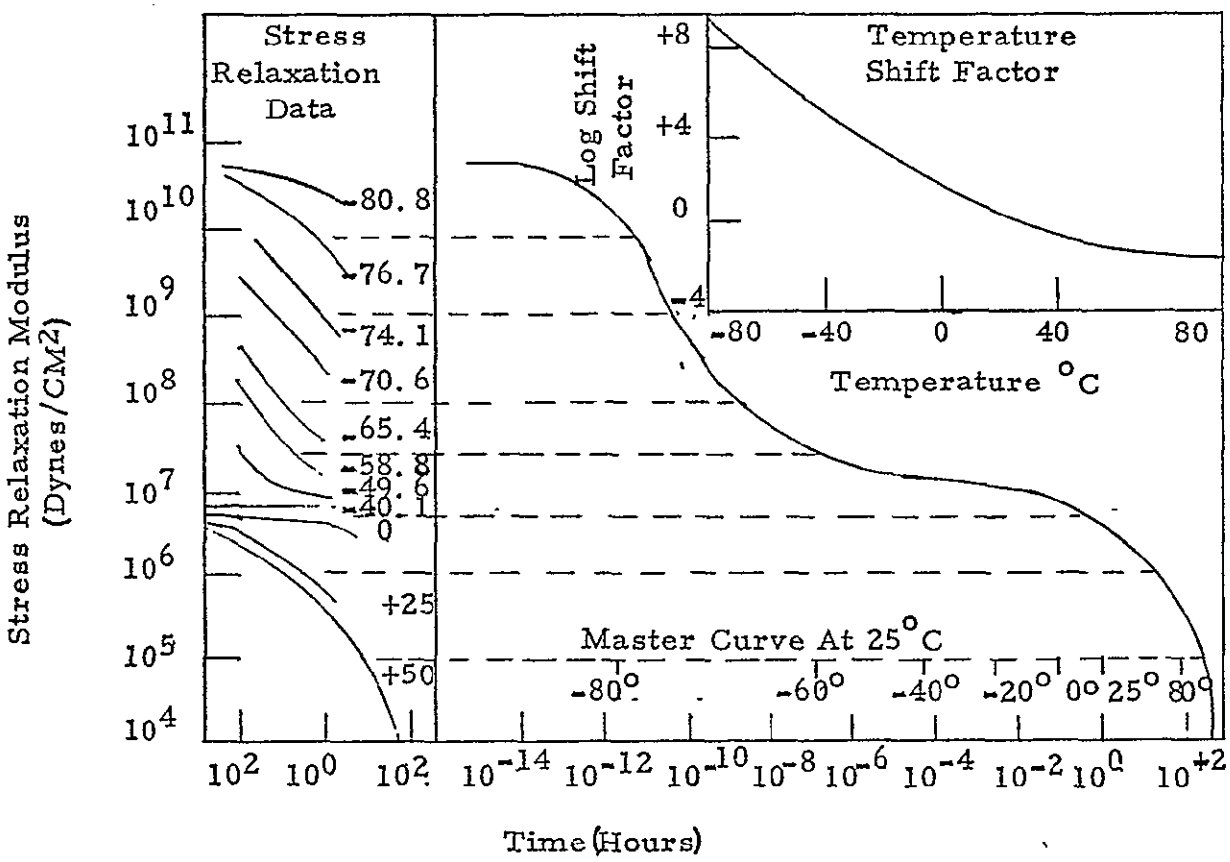

Figure A-11. Time-Temperature Shift Principal

3.3.7 Effects of Frequency

The theoretical development of the dynamic moduli showed them to be functions of frequency. A master curve of dynamic shear moduli for a viscoelastic material is shown in Figure A-12. It is seen that the moduli increase with frequency at first and then decrease as the frequency is further increased.

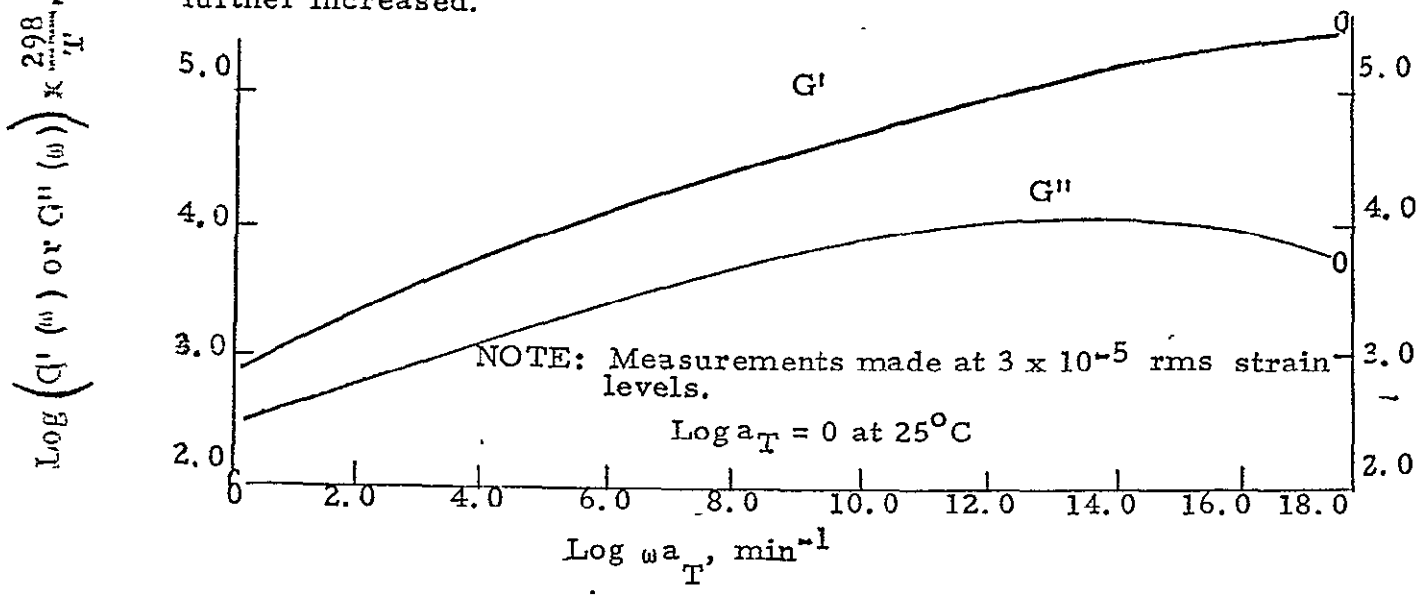

Figure A-12. Frequency Effect on Dynamic Shear Moduli

3.3.8 Effects of Strain

An increase in strain has been found to decrease the dynamic moduli (Reference 9). The variation is shown for typical viscoelastic materials in Figure A-13 and Figure A-14.

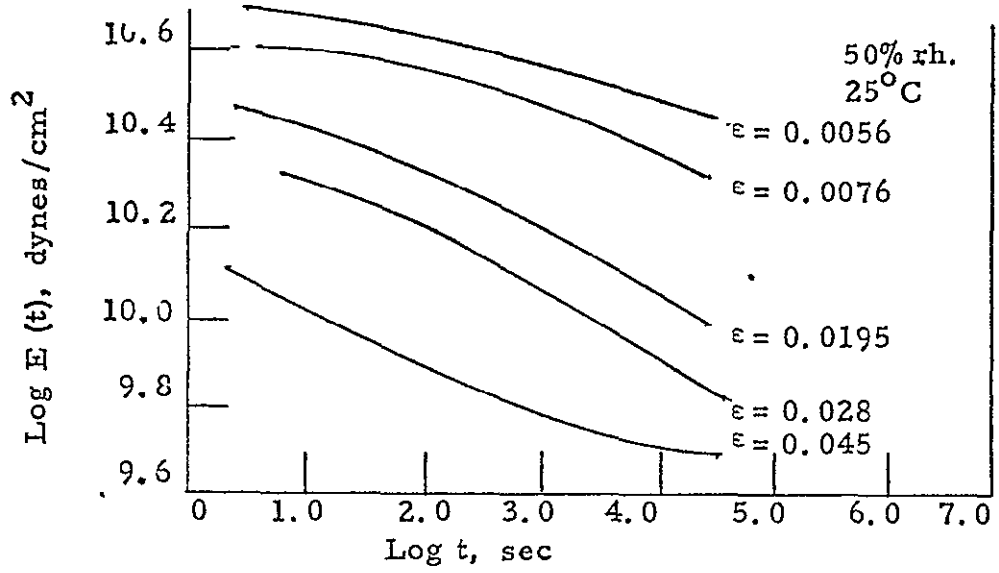

Figure A-13. Effects of Strain on Relaxation Modulus

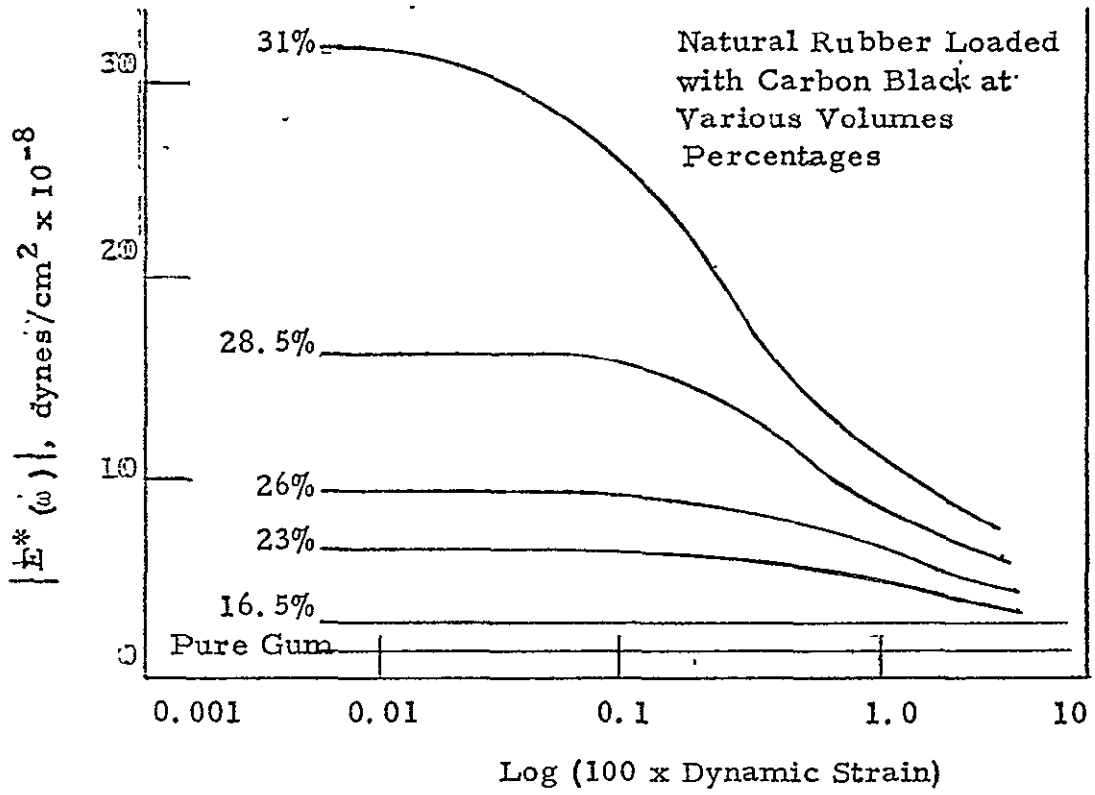

Figure A-14. Absolute Elastic Modulus vs. Amplitude of Sinusoidal Strain at 0.5 cps

3.3.9 Effects of Pressure

An increase in pressure has also been shown to increase the dynamic moduli. Figure A-15 shows the increase in the relaxation modulus with an increase in pressure from ambient to 1000 psi. The operational pressure of the SRB will be near 1000 psi.

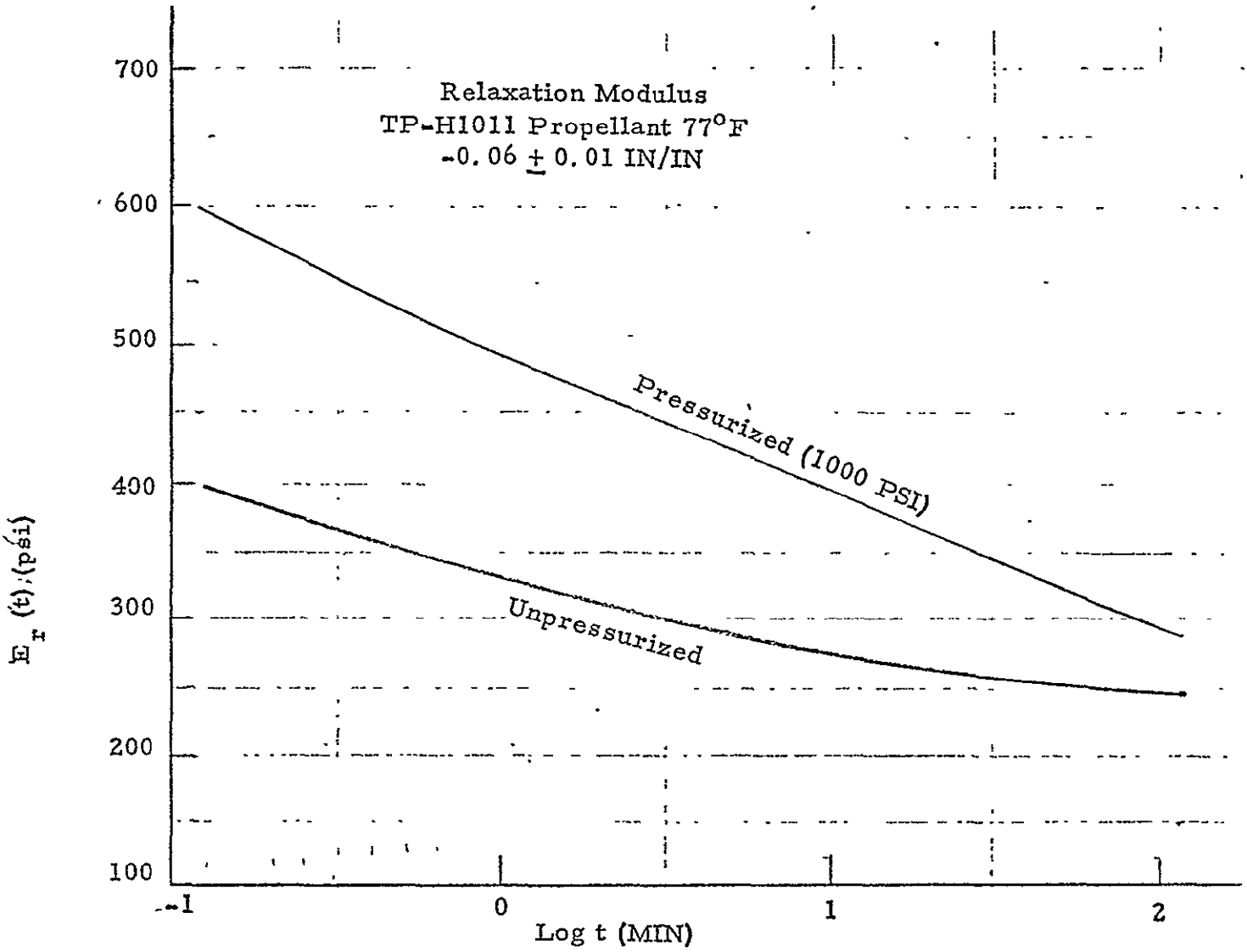

Figure A-15. Influence of Pressure on Relaxation Modulus

3.3.10 Effects of Temperature

A decrease in temperature causes an increase in the dynamic modulus. The increase in the relaxation modulus as temperature decreases is shown in Figure A-11. Due to the rapid burning rate and the low thermal conductivity of the propellant, the temperature of the propellant will not increase significantly during its flight. Therefore, the temperature used for dynamic analysis should be the ambient temperature.

4.0 SUMMARY

The physical properties of viscoelastic materials required for dynamic analysis has been defined and characterized. These properties are elastic modulus, shear modulus, Poisson's ratio and the damping ratio. It was found that viscoelastic materials are incompressible and therefore Poisson's ratio is 0.5. It was also found that the dynamic elastic modulus and the dynamic shear modulus are complex and can be represented in the following form.

$$E(\omega) = E'(\omega) + E''(\omega) \tag{47}$$

and

$$G(\omega) = G'(\omega) + G''(\omega) \tag{48}$$

It was shown that $E'(\omega)$ and $E''(\omega)$ could be determined from the time response to a step strain, $E_r(t)$, or $G'(\omega)$ and $G''(\omega)$ could be determined by measuring the response of a vibrating disk. Dynamic shear modulus and dynamic elastic modulus are related by

$$E(\omega) = 3G(\omega) \tag{49}$$

The damping ratio, δ, was found to be

$$\delta = \frac{E''}{2E'} \tag{50}$$

The dependence of the storage moduli and the loss moduli on frequency, strain, pressure, and temperature were discussed. All of these effects must be considered during a dynamic analysis.

APPENDIX B

NASTRAN COMPUTER MODEL

APPENDIX B

NASTRAN Computer Model

The trapezoidal ring element is used to generate an axisymmetric model of a hollow cylinder to evaluate the thickness shear mode. The propellant is represented by a 10 x 10 grid as shown in Figure B-1. The z dimensions of the ring elements are varied to obtain cylinders of different lengths.

For data card preparation, only the cards which are different than those for normal mode analysis will be discussed. As mentioned previously, rigid format seven or ten can be used. In rigid format seven, the displacements of the grid points are used as the degrees of freedom, and in rigid format ten the normal vibration modes of the undamped system are used as the degrees of freedom.

The METHOD card, which specifies an EIGR card in normal mode analysis, must be replaced by a CMETHOD card which specifies an EIGC card. The EIGC card selects the method for eigenvalue extraction and the search region. The specification of the search region was found to be the most critical area in complex eigenvalue analysis. If the search region is not specified with some degree of reasonableness, the computer time to extract the roots can become excessive or they cannot be found at all. The eigenvalue lies in the complex plane. Better results are obtained when a normal eigenvalue analysis is first made and an estimate is made of the decay rate based on the amount of damping. A typical search region is shown in Figure B-2. It is important to note that the search region for a system with less than critical damping lies in the second quadrant.

The complex stiffness is calculated by NASTRAN by two different methods. All elements can be given equal damping by specifying G on a PARAM card or each element can be given a different value of damping by specifying GE on the element's material property card. Viscous damping can be specified by using a scalar damper or a viscous rod element.

One other property which must be input is Poisson's ratio. As mentioned previously Poisson's ratio for viscoelastic materials is 0.5. NASTRAN cannot accept this value due to a 1-2 ν term in the denominator of some equations. For this reason a value of 0.495 is used. It is interesting to note that in the thickness shear mode motion only occurs in one direction, therefore, Poisson's ratio does not appear in the differential equations of motion. Computer runs were also made using a Poisson's ratio of 0.3. The eigenvalues did change by a small percentage probably due to radial motion still present in the computer model.

A sample NASTRAN listing is given in Attachment.

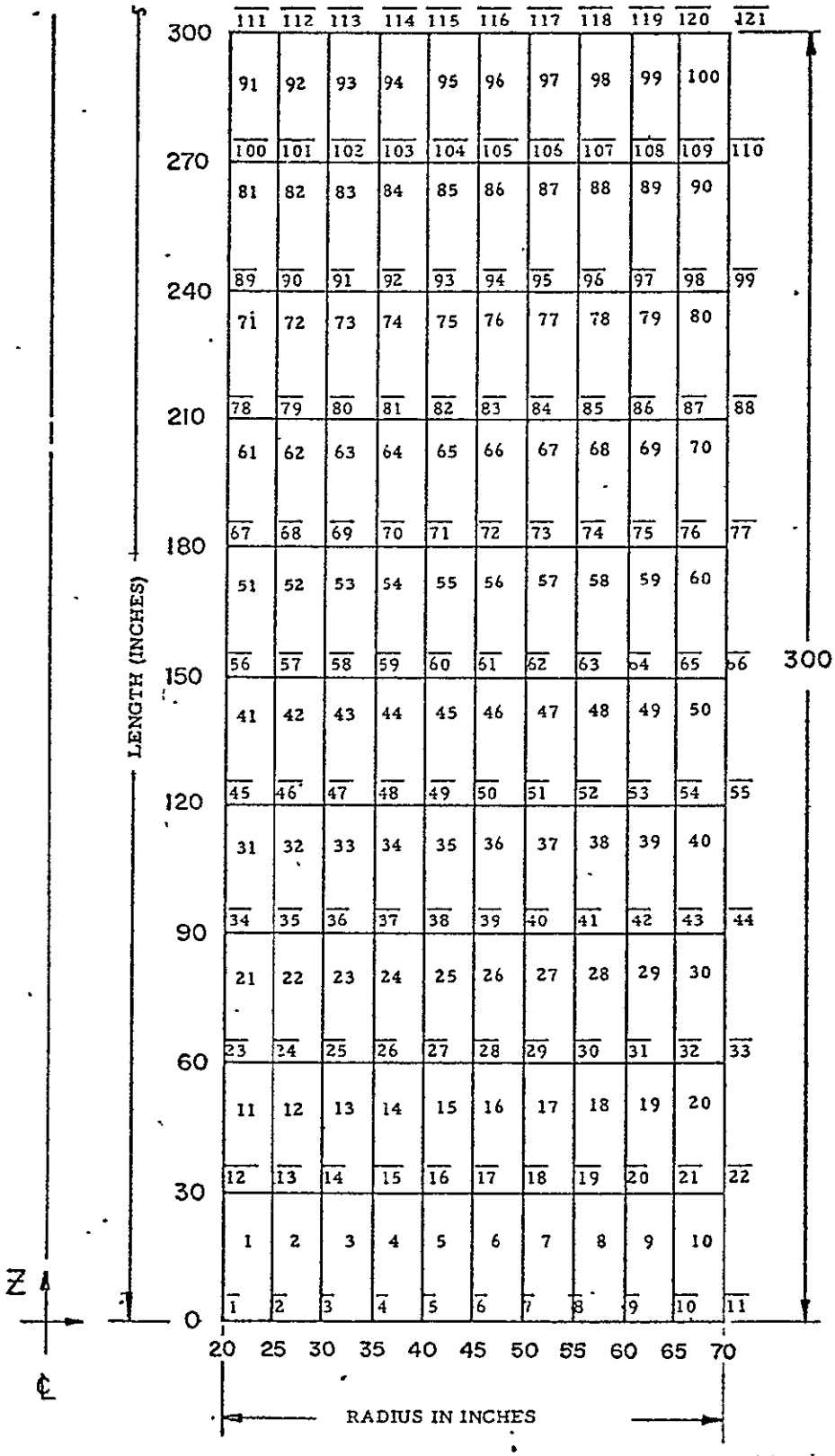

FIGURE B-1. Computer Model

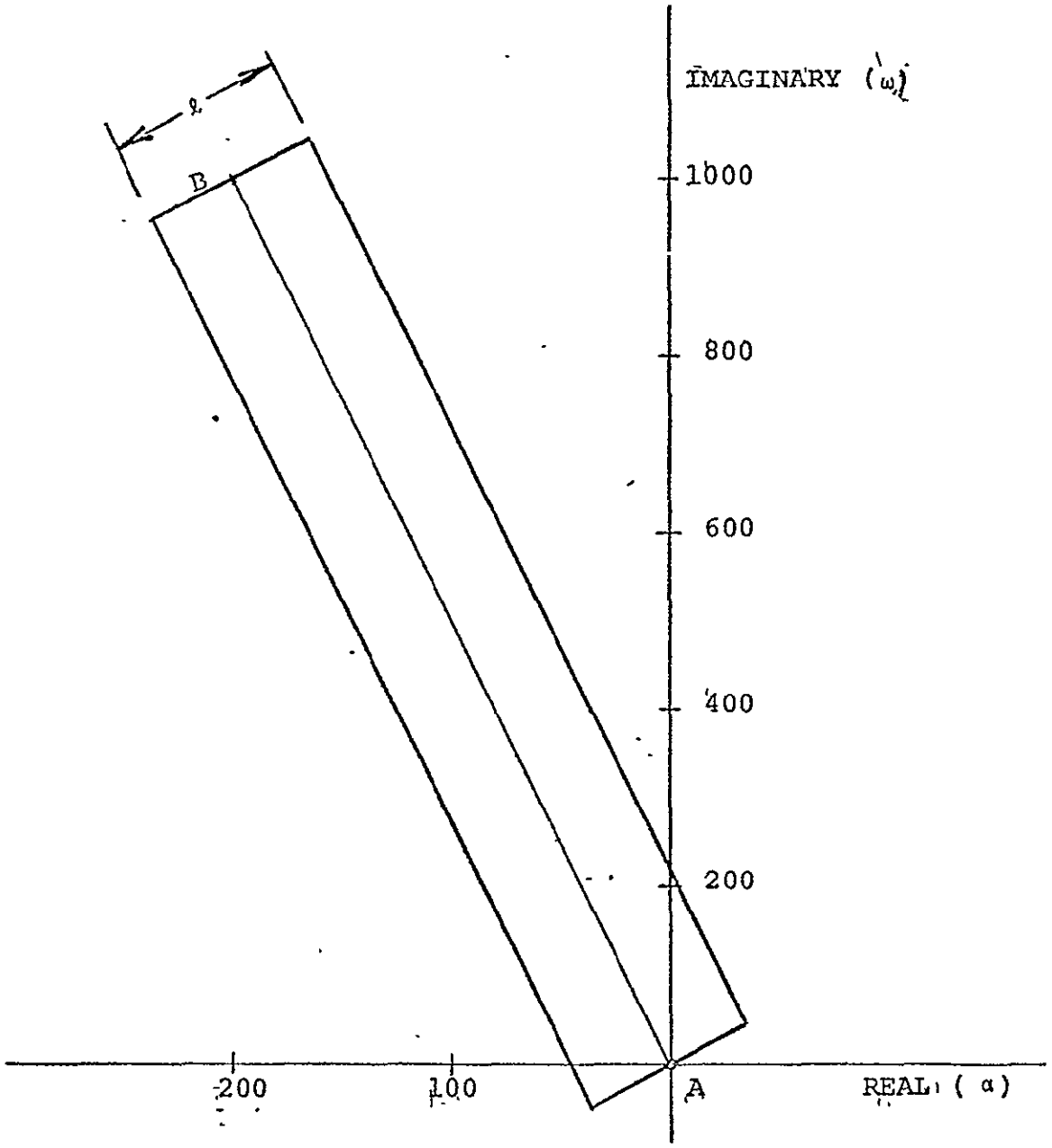

Figure B-2. Search Region

APPENDIX B ATTACHMENT

N A S T R A N E X E C U T I V E C O N T R O L D E C K E C H O

```
ID SRB LONGITUDINAL SHEAR ANALYSIS
APP DISPLACEMENT
TIME 10
SOL 7,0
CEND
```

CASE CONTROL DECK ECHO

CARD COUNT	
1	TITLE # NORMAL MODE ANALYSIS
2	SPC#30
3	CMETHOD#11
4	DISPLACEMENT#ALL
5	BEGIN BULK

SORTED BULK DATA ECHO

CARD COUNT	1	2	3	4	5	6	7	8	9	10
1-	CTRAPRG 1	1	2	13	12		20			
2-	CTRAPRG 2	2	3	14	13		20			
3-	CTRAPRG 3	3	4	15	14		20			
4-	CTRAPRG 4	4	5	16	15		20			
5-	CTRAPRG 5	5	6	17	16		20			
6-	CTRAPRG 6	6	7	18	17		20			
7-	CTRAPRG 7	7	8	19	18		20			
8-	CTRAPRG 8	8	9	20	19		20			
9-	CTRAPRG 9	9	10	21	20		20			
10-	CTRAPRG 10	10	11	22	21		20			
11-	CTRAPRG 11	12	13	24	23		20			
12-	CTRAPRG 12	13	14	25	24		20			
13-	CTRAPRG 13	14	15	26	25		20			
14-	CTRAPRG 14	15	16	27	26		20			
15-	CTRAPRG 15	16	17	28	27		20			
16-	CTRAPRG 16	17	18	29	28		20			
17-	CTRAPRG 17	18	19	30	29		20			
18-	CTRAPRG 18	19	20	31	30		20			
19-	CTRAPRG 19	20	21	32	31		20			
20-	CTRAPRG 20	21	22	33	32		20			
21-	CTRAPRG 21	23	24	35	34		20			
22-	CTRAPRG 22	24	25	36	35		20			
23-	CTRAPRG 23	25	26	37	36		20			
24-	CTRAPRG 24	26	27	38	37		20			
25-	CTRAPRG 25	27	28	39	38		20			
26-	CTRAPRG 26	28	29	40	39		20			
27-	CTRAPRG 27	29	30	41	40		20			
28-	CTRAPRG 28	30	31	42	41		20			
29-	CTRAPRG 29	31	32	43	42		20			
30-	CTRAPRG 30	32	33	44	43		20			
31-	CTRAPRG 31	34	35	46	45		20			
32-	CTRAPRG 32	35	36	47	46		20			
33-	CTRAPRG 33	36	37	48	47		20			
34-	CTRAPRG 34	37	38	49	48		20			
35-	CTRAPRG 35	38	39	50	49		20			
36-	CTRAPRG 36	39	40	51	50		20			
37-	CTRAPRG 37	40	41	52	51		20			
38-	CTRAPRG 38	41	42	53	52		20			
39-	CTRAPRG 39	42	43	54	53		20			
40-	CTRAPRG 40	43	44	55	54		20			
41-	CTRAPRG 41	45	46	57	56		20			
42-	CTRAPRG 42	46	47	58	57		20			
43-	CTRAPRG 43	47	48	59	58		20			
44-	CTRAPRG 44	48	49	60	59		20			
45-	CTRAPRG 45	49	50	61	60		20			
46-	CTRAPRG 46	50	51	62	61		20			
47-	CTRAPRG 47	51	52	63	62		20			
48-	CTRAPRG 48	52	53	64	63		20			
49-	CTRAPRG 49	53	54	65	64		20			
50-	CTRAPRG 50	54	55	66	65		20			

SORTED BULK DATA ECHO

CARD COUNT	1	2	3	4	5	6	7	8	9	10
51-	CTRAPRG	51	56	57	68	67		20		
52-	CTRAPRG	52	57	58	69	68		20		
53-	CTRAPRG	53	58	59	70	69		20		
54-	CTRAPRG	54	59	60	71	70		20		
55-	CTRAPRG	55	60	61	72	71		20		
56-	CTRAPRG	56	61	62	73	72		20		
57-	CTRAPRG	57	62	63	74	73		20		
58-	CTRAPRG	58	63	64	75	74		20		
59-	CTRAPRG	59	64	65	76	75		20		
60-	CTRAPRG	60	65	66	77	76		20		
61-	CTRAPRG	61	67	68	79	78		20		
62-	CTRAPRG	62	68	69	80	79		20		
63-	CTRAPRG	63	69	70	81	80		20		
64-	CTRAPRG	64	70	71	82	81		20		
65-	CTRAPRG	65	71	72	83	82		20		
66-	CTRAPRG	66	72	73	84	83		20		
67-	CTRAPRG	67	73	74	85	84		20		
68-	CTRAPRG	68	74	75	86	85		20		
69-	CTRAPRG	69	75	76	87	86		20		
70-	CTRAPRG	70	76	77	88	87		20		
71-	CTRAPRG	71	78	79	90	89		20		
72-	CTRAPRG	72	79	80	91	90		20		
73-	CTRAPRG	73	80	81	92	91		20		
74-	CTRAPRG	74	81	82	93	92		20		
75-	CTRAPRG	75	82	83	94	93		20		
76-	CTRAPRG	76	83	84	95	94		20		
77-	CTRAPRG	77	84	85	96	95		20		
78-	CTRAPRG	78	85	86	97	96		20		
79-	CTRAPRG	79	86	87	98	97		20		
80-	CTRAPRG	80	87	88	99	98		20		
81-	CTRAPRG	81	89	90	101	100		20		
82-	CTRAPRG	82	90	91	102	101		20		
83-	CTRAPRG	83	91	92	103	102		20		
84-	CTRAPRG	84	92	93	104	103		20		
85-	CTRAPRG	85	93	94	105	104		20		
86-	CTRAPRG	86	94	95	106	105		20		
87-	CTRAPRG	87	95	96	107	106		20		
88-	CTRAPRG	88	96	97	108	107		20		
89-	CTRAPRG	89	97	98	109	108		20		
90-	CTRAPRG	90	98	99	110	109		20		
91-	CTRAPRG	91	100	101	112	111		20		
92-	CTRAPRG	92	101	102	113	112		20		
93-	CTRAPRG	93	102	103	114	113		20		
94-	CTRAPRG	94	103	104	115	114		20		
95-	CTRAPRG	95	104	105	116	115		20		
96-	CTRAPRG	96	105	106	117	116		20		
97-	CTRAPRG	97	106	107	118	117		20		
98-	CTRAPRG	98	107	108	119	118		20		
99-	CTRAPRG	99	108	109	120	119		20		
100-	CTRAPRG	100	109	110	121	120		20		

S O R T E D B U L K D A T A E C H O

CARD COUNT	1	2	3	4	5	6	7	8	9	10
101-	FIGC	11	INV	MAX						ABC1
102-	&BC1	-30.0	190.0	-30.0	240.0	20.0	1	1		ABC2
103-	&BC2	-92.0	500.0	-92.0	550.0	20.0	1	1		ABC3
104-	&BC3	-104.0	590.0	-104.0	640.0	20.0	1	1		ABC4
105-	&BC4	-338.0	760.0	-138.0	810.0	20.0	1	1		ABC5
106-	&BC5	-180.0	995.0	-180.0	1045.0	20.0	1	1		
107-	GRDSET						2456			
108-	GRID	1		20.	0.0	0.0				
109-	GRID	2		25.	0.0	0.0				
110-	GRID	3		30.	0.0	0.0				
111-	GRID	4		35.	0.0	0.0				
112-	GRID	5		40.	0.0	0.0				
113-	GRID	6		45.	0.0	0.0				
114-	GRID	7		50.	0.0	0.0				
115-	GRID	8		55.	0.0	0.0				
116-	GRID	9		60.	0.0	0.0				
117-	GRID	10		65.	0.0	0.0				
118-	GRID	11		70.	0.0	0.0				
119-	GRID	12		20.	0.0	30.				
120-	GRID	13		25.	0.0	30.				
121-	GRID	14		30.	0.0	30.				
122-	GRID	15		35.	0.0	30.				
123-	GRID	16		40.	0.0	30.				
124-	GRID	17		45.	0.0	30.				
125-	GRID	18		50.	0.0	30.				
126-	GRID	19		55.	0.0	30.				
127-	GRID	20		60.	0.0	30.				
128-	GRID	21		65.	0.0	30.				
129-	GRID	22		70.	0.0	30.				
130-	GRID	23		20.	0.0	60.				
131-	GRID	24		25.	0.0	60.				
132-	GRID	25		30.	0.0	60.				
133-	GRID	26		35.	0.0	60.				
134-	GRID	27		40.	0.0	60.				
135-	GRID	28		45.	0.0	60.				
136-	GRID	29		50.	0.0	60.				
137-	GRID	30		55.	0.0	60.				
138-	GRID	31		60.	0.0	60.				
139-	GRID	32		65.	0.0	60.				
140-	GRID	33		70.	0.0	60.				
141-	GRID	34		20.	0.0	90.				
142-	GRID	35		25.	0.0	90.				
143-	GRID	36		30.	0.0	90.				
144-	GRID	37		35.	0.0	90.				
145-	GRID	38		40.	0.0	90.				
146-	GRID	39		45.	0.0	90.				
147-	GRID	40		50.	0.0	90.				
148-	GRID	41		55.	0.0	90.				
149-	GRID	42		60.	0.0	90.				
150-	GRID	43		65.	0.0	90.				

SORTED BULK DATA ECHO

CARD COUNT	1	2	3	4	5	6	7	8	9	10
151-	GRID	44		70.	0.0	90.				
152-	GRID	45		20.	0.0	120.				
153-	GRID	46		25.	0.0	120.				
154-	GRID	47		30.	0.0	120.				
155-	GRID	48		35.	0.0	120.				
156-	GRID	49		40.	0.0	120.				
157-	GRID	50		45.	0.0	120.				
158-	GRID	51		50.	0.0	120.				
159-	GRID	52		55.	0.0	120.				
160-	GRID	53		60.	0.0	120.				
161-	GRID	54		65.	0.0	120.				
162-	GRID	55		70.	0.0	120.				
163-	GRID	56		20.	0.0	150.				
164-	GRID	57		25.	0.0	150.				
165-	GRID	58		30.	0.0	150.				
166-	GRID	59		35.	0.0	150.				
167-	GRID	60		40.	0.0	150.				
168-	GRID	61		45.	0.0	150.				
169-	GRID	62		50.	0.0	150.				
170-	GRID	63		55.	0.0	150.				
171-	GRID	64		60.	0.0	150.				
172-	GRID	65		65.	0.0	150.				
173-	GRID	66		70.	0.0	150.				
174-	GRID	67		20.	0.0	180.				
175-	GRID	68		25.	0.0	180.				
176-	GRID	69		30.	0.0	180.				
177-	GRID	70		35.	0.0	180.				
178-	GRID	71		40.	0.0	180.				
179-	GRID	72		45.	0.0	180.				
180-	GRID	73		50.	0.0	180.				
181-	GRID	74		55.	0.0	180.				
182-	GRID	75		60.	0.0	180.				
183-	GRID	76		65.	0.0	180.				
184-	GRID	77		70.	0.0	180.				
185-	GRID	78		20.	0.0	210.				
186-	GRID	79		25.	0.0	210.				
187-	GRID	80		30.	0.0	210.				
188-	GRID	81		35.	0.0	210.				
189-	GRID	82		40.	0.0	210.				
190-	GRID	83		45.	0.0	210.				
191-	GRID	84		50.	0.0	210.				
192-	GRID	85		55.	0.0	210.				
193-	GRID	86		60.	0.0	210.				
194-	GRID	87		65.	0.0	210.				
195-	GRID	88		70.	0.0	210.				
196-	GRID	89		20.	0.0	240.				
197-	GRID	90		25.	0.0	240.				
198-	GRID	91		30.	0.0	240.				
199-	GRID	92		35.	0.0	240.				
200-	GRID	93		40.	0.0	240.				

SORTED BULK DATA ECHO

```
CARD
COUNT     .  1  ..  2  ..  3  ..  4  ..  5  ..  6  ..  7  ..  8  ..  9  .. 10  .
  201-    GRID    94              45.     0.0     240.
  202-    GRID    95              50.     0.0     240.
  203-    GRID    96              55.     0.0     240.
  204-    GRID    97              60.     0.0     240.
  205-    GRID    98              65.     0.0     240.
  206-    GRID    99              70.     0.0     240.
  207-    GRID    100             20.     0.0     270.
  208-    GRID    101             25.     0.0     270.
  209-    GRID    102             30.     0.0     270.
  210-    GRID    103             35.     0.0     270.
  211-    GRID    104             40.     0.0     270.
  212-    GRID    105             45.     0.0     270.
  213-    GRID    106             50.     0.0     270.
  214-    GRID    107             55.     0.0     270.
  215-    GRID    108             60.     0.0     270.
  216-    GRID    109             65.     0.0     270.
  217-    GRID    110             70.     0.0     270.
  218-    GRID    111             20.     0.0     300.
  219-    GRID    112             25.     0.0     300.
  220-    GRID    113             30.     0.0     300.
  221-    GRID    114             35.     0.0     300.
  222-    GRID    115             40.     0.0     300.
  223-    GRID    116             45.     0.0     300.
  224-    GRID    117             50.     0.0     300.
  225-    GRID    118             55.     0.0     300.
  226-    GRID    119             60.     0.0     300.
  227-    GRID    120             65.     0.0     300.
  228-    GRID    121             70.     0.0     300.
  229-    MAT1    20              6244.0  0.495   1.658E-4                        0.364
  230-    PARAM   COUPMASS1
  231-    SPC1    30      13      11      22      33      44      55      66      XYZ1
  232-    &YZ1            77      88      99      110     121
          ENDDATA
```

NO ERRORS FOUND - EXECUTE NASTRAN PROGRAM

***USER INFORMATION MESSAGE 3023,

***USER INFORMATION MESSAGE 3028,

BBAR # 23 CBAR # 0 R # 46

DECOMPOSITION TIME ESTIMATE IS 1

C O M P L E X E I G E N V A L U E A N A L Y S I S S U M M A R Y %INVERSE POWER WITH SHIFTS<

NUMBER OF EIGENVALUES EXTRACTED	1
NUMBER OF STARTING POINTS USED	1
NUMBER OF STARTING POINT OR SHIFT POINT MOVES . .	0
TOTAL NUMBER OF TRIANGULAR DECOMPOSITIONS	1
TOTAL NUMBER OF VECTOR ITERATIONS	10
REASON FOR TERMINATION	6

COMPLEX EIGENVALUE SUMMARY

ROOT NO.	EXTRACTION ORDER	EIGENVALUE %REAL<	EIGENVALUE %IMAG<	FREQUENCY %CYCLES<	DAMPING COEFFICIENT
1	1	-4.299365E 01	2.438104E 02	3.880362E 01	3.526810E-01
2	2	-8.961200E 01	5.081758E 02	8.087868E 01	3.526811E-01
3	3	-1.046121E 02	5.932393E 02	9.441696E 01	3.526810E-01
4	4	-1.450609E 02	8.226182E 02	1.309238E 02	3.526810E-01
5	5	-1.800453E 02	1.021009E 03	1.624987E 02	3.526810E-01

COMPLEX EIGENVALUE # -4.299365E 01, 2.438104E 02

COMPLEX EIGENVECTOR NO. 1

%REAL/IMAGINARY<

POINT ID.	TYPE	T1	T2	T3	R1	R2	R3
1	G	-1.218973E-01	0.0	9.805287E-01	0.0	0.0	0.0
		6.469871E-07	0.0	-3.207562E-07	0.0	0.0	0.0
2	G	-1.008059E-01	0.0	9.631643E-01	0.0	0.0	0.0
		4.763742E-07	0.0	-5.123048E-07	0.0	0.0	0.0
3	G	-8.555853E-02	0.0	9.144636E-01	0.0	0.0	0.0
		3.468022E-07	0.0	-5.682792E-07	0.0	0.0	0.0
4	G	-7.362592E-02	0.0	8.434793E-01	0.0	0.0	0.0
		2.475405E-07	0.0	-5.456513E-07	0.0	0.0	0.0
5	G	-6.309706E-02	0.0	7.545497E-01	0.0	0.0	0.0
		1.704041E-07	0.0	-4.696535E-07	0.0	0.0	0.0
6	G	-5.282917E-02	0.0	6.511883E-01	0.0	0.0	0.0
		1.107600E-07	0.0	-3.607460E-07	0.0	0.0	0.0
7	G	-4.217958E-02	0.0	5.365742E-01	0.0	0.0	0.0
		6.585117E-08	0.0	-2.386519E-07	0.0	0.0	0.0
8	G	-3.089758E-02	0.0	4.135358E-01	0.0	0.0	0.0
		3.386248E-08	0.0	-1.229655E-07	0.0	0.0	0.0
9	G	-1.915107E-02	0.0	2.841575E-01	0.0	0.0	0.0
		1.334267E-08	0.0	-3.272350E-08	0.0	0.0	0.0
10	G	-7.735811E-03	0.0	1.488124E-01	0.0	0.0	0.0
		2.772419E-09	0.0	1.406336E-08	0.0	0.0	0.0
11	G	0.0	0.0	0.0	0.0	0.0	0.0
		0.0	0.0	0.0	0.0	0.0	0.0
12	G	-2.562813E-02	0.0	1.000000E 00	0.0	0.0	0.0
		8.326465E-07	0.0	0.0	0.0	0.0	0.0
13	G	-2.130374E-02	0.0	9.709264E-01	0.0	0.0	0.0
		6.007166E-07	0.0	-1.073025E-07	0.0	0.0	0.0
14	G	-1.815515E-02	0.0	9.174005E-01	0.0	0.0	0.0
		4.311067E-07	0.0	-1.630101E-07	0.0	0.0	0.0
15	G	-1.551128E-02	0.0	8.405590E-01	0.0	0.0	0.0
		3.017041E-07	0.0	-1.662753E-07	0.0	0.0	0.0
16	G	-1.298326E-02	0.0	7.444257E-01	0.0	0.0	0.0
		2.018667E-07	0.0	-1.320381E-07	0.0	0.0	0.0

COMPLEX EIGENVALUE # -4.299365E 01, 2.438104E 02

COMPLEX EIGENVECTOR NO. 1

%REAL/IMAGINARY<

POINT ID.	TYPE	T1	T2	T3	R1	R2	R3
17	G	-1.033861E-02	0.0	6.330248E-01	0.0	0.0	0.0
		1.257787E-07	0.0	-7.577830E-08	0.0	0.0	0.0
18	G	-7.501747E-03	0.0	5.104187E-01	0.0	0.0	0.0
		6.992326E-08	0.0	-1.351583E-08	0.0	0.0	0.0
19	G	-4.560620E-03	0.0	3.807130E-01	0.0	0.0	0.0
		3.177631E-08	0.0	3.886636E-08	0.0	0.0	0.0
20	G	-1.812063E-03	0.0	2.481694E-01	0.0	0.0	0.0
		9.097075E-09	0.0	6.649805E-08	0.0	0.0	0.0
21	G	7.491151E-05	0.0	1.174533E-01	0.0	0.0	0.0
		-5.152405E-10	0.0	5.659170E-08	0.0	0.0	0.0
22	G	0.0	0.0	0.0	0.0	0.0	0.0
		0.0	0.0	0.0	0.0	0.0	0.0
23	G	-3.145144E-03	0.0	9.923275E-01	0.0	0.0	0.0
		1.268146E-06	0.0	6.432858E-07	0.0	0.0	0.0
24	G	-1.049328E-03	0.0	9.687438E-01	0.0	0.0	0.0
		9.071106E-07	0.0	5.256587E-07	0.0	0.0	0.0
25	G	-3.896000E-05	0.0	9.149157E-01	0.0	0.0	0.0
		6.491471E-07	0.0	4.529155E-07	0.0	0.0	0.0
26	G	5.926276E-04	0.0	8.372628E-01	0.0	0.0	0.0
		4.543343E-07	0.0	4.047499E-07	0.0	0.0	0.0
27	G	1.019964E-03	0.0	7.399346E-01	0.0	0.0	0.0
		3.046951E-07	0.0	3.733484E-07	0.0	0.0	0.0
28	G	1.291800E-03	0.0	6.273241E-01	0.0	0.0	0.0
		1.908630E-07	0.0	3.489028E-07	0.0	0.0	0.0
29	G	1.398894E-03	0.0	5.039493E-01	0.0	0.0	0.0
		1.072219E-07	0.0	3.211370E-07	0.0	0.0	0.0
30	G	1.289513E-03	0.0	3.745328E-01	0.0	0.0	0.0
		4.976563E-08	0.0	2.800233E-07	0.0	0.0	0.0
31	G	8.899502E-04	0.0	2.440590E-01	0.0	0.0	0.0
		1.504150E-08	0.0	2.167030E-07	0.0	0.0	0.0
32	G	2.198874E-04	0.0	1.164155E-01	0.0	0.0	0.0
		-3.703391E-10	0.0	1.244841E-07	0.0	0.0	0.0

COMPLEX EIGENVALUE # -4.299365E 01, 2.438104E 02

COMPLEX EIGENVECTOR NO. 1

%REAL/IMAGINARY<

POINT ID.	TYPE	T1	T2	T3	R1	R2	R3
33	G	0.0	0.0	0.0	0.0	0.0	0.0
		0.0	0.0	0.0	0.0	0.0	0.0
34	G	1.149066E-03	0.0	9.794863E-01	0.0	0.0	0.0
		1.682043E-06	0.0	1.554316E-06	0.0	0.0	0.0
35	G	2.395362E-03	0.0	9.597986E-01	0.0	0.0	0.0
		1.205703E-06	0.0	1.436731E-06	0.0	0.0	0.0
36	G	3.114589E-03	0.0	9.090770E-01	0.0	0.0	0.0
		8.630889E-07	0.0	1.324816E-06	0.0	0.0	0.0
37	G	3.385860E-03	0.0	8.333428E-01	0.0	0.0	0.0
		6.046262E-07	0.0	1.209190E-06	0.0	0.0	0.0
38	G	3.330474E-03	0.0	7.377120E-01	0.0	0.0	0.0
		4.062583E-07	0.0	1.084350E-06	0.0	0.0	0.0
39	G	2.999298E-03	0.0	6.267717E-01	0.0	0.0	0.0
		2.553075E-07	0.0	9.471724E-07	0.0	0.0	0.0
40	G	2.428752E-03	0.0	5.051230E-01	0.0	0.0	0.0
		1.441755E-07	0.0	7.947182E-07	0.0	0.0	0.0
41	G	1.675395E-03	0.0	3.774077E-01	0.0	0.0	0.0
		6.749576E-08	0.0	6.245563E-07	0.0	0.0	0.0
42	G	8.615635E-04	0.0	2.482598E-01	0.0	0.0	0.0
		2.076525E-08	0.0	4.352262E-07	0.0	0.0	0.0
43	G	2.602155E-04	0.0	1.213872E-01	0.0	0.0	0.0
		-3.023306E-10	0.0	2.266545E-07	0.0	0.0	0.0
44	G	0.0	0.0	0.0	0.0	0.0	0.0
		0.0	0.0	0.0	0.0	0.0	0.0
45	G	8.191620E-04	0.0	9.708875E-01	0.0	0.0	0.0
		1.963525E-06	0.0	2.654735E-06	0.0	0.0	0.0
46	G	1.449163E-03	0.0	9.525841E-01	0.0	0.0	0.0
		1.409411E-06	0.0	2.556211E-06	0.0	0.0	0.0
47	G	1.858214E-03	0.0	9.039427E-01	0.0	0.0	0.0
		1.009693E-06	0.0	2.404514E-06	0.0	0.0	0.0
48	G	2.026225E-03	0.0	8.303879E-01	0.0	0.0	0.0
		7.073825E-07	0.0	2.205611E-06	0.0	0.0	0.0

COMPLEX EIGENVALUE # -4.299365E 01, 2.438104E 02

COMPLEX EIGENVECTOR NO. 1

%REAL/IMAGINARY<

POINT ID.	TYPE	T1	T2	T3	R1	R2	R3
49	G	1.962661E-03	0.0	7.367498E-01	0.0	0.0	0.0
		4.752676E-07	0.0	1.965017E-06	0.0	0.0	0.0
50	G	1.706339E-03	0.0	6.276329E-01	0.0	0.0	0.0
		2.986976E-07	0.0	1.600483E-06	0.0	0.0	0.0
51	G	1.306089E-03	0.0	5.074988E-01	0.0	0.0	0.0
		1.687405E-07	0.0	1.382300E-06	0.0	0.0	0.0
52	G	8.366492E-04	0.0	3.807095E-01	0.0	0.0	0.0
		7.906692E-08	0.0	1.053110E-06	0.0	0.0	0.0
53	G	4.088294E-04	0.0	2.513349E-01	0.0	0.0	0.0
		2.438256E-08	0.0	7.079468E-07	0.0	0.0	0.0
54	G	1.075936E-04	0.0	1.232286E-01	0.0	0.0	0.0
		-2.843490E-10	0.0	3.542937E-07	0.0	0.0	0.0
55	G	0.0	0.0	0.0	0.0	0.0	0.0
		0.0	0.0	0.0	0.0	0.0	0.0
56	G	-3.939645E-06	0.0	9.680140E-01	0.0	0.0	0.0
		2.060445E-06	0.0	3.864448E-06	0.0	0.0	0.0
57	G	-2.825185E-06	0.0	9.500389E-01	0.0	0.0	0.0
		1.477583E-06	0.0	3.792674E-06	0.0	0.0	0.0
58	G	-2.020747E-06	0.0	9.020468E-01	0.0	0.0	0.0
		1.056863E-06	0.0	3.601053E-06	0.0	0.0	0.0
59	G	-1.412485E-06	0.0	8.293083E-01	0.0	0.0	0.0
		7.387416E-07	0.0	3.310635E-06	0.0	0.0	0.0
60	G	-9.461629E-07	0.0	7.364896E-01	0.0	0.0	0.0
		4.948533E-07	0.0	2.940058E-06	0.0	0.0	0.0
61	G	-5.925094E-07	0.0	6.280836E-01	0.0	0.0	0.0
		3.098906E-07	0.0	2.507265E-06	0.0	0.0	0.0
62	G	-3.332933E-07	0.0	5.084775E-01	0.0	0.0	0.0
		1.743184E-07	0.0	2.029777E-06	0.0	0.0	0.0
63	G	-1.552484E-07	0.0	3.818755E-01	0.0	0.0	0.0
		8.119872E-08	0.0	1.524380E-06	0.0	0.0	0.0
64	G	-4.728210E-08	0.0	2.523409E-01	0.0	0.0	0.0
		2.473050E-08	0.0	1.007290E-06	0.0	0.0	0.0

COMPLEX EIGENVALUE # -4.299365E 01, 2.438104E 02

COMPLEX EIGENVECTOR NO. 1

%REAL/IMAGINARY%

POINT ID.	TYPE	T1	T2	T3	R1	R2	R3
65	G	1.039009E-09	0.0	1.237865E-01	0.0	0.0	0.0
		-5.427849E-10	0.0	4.941268E-07	0.0	0.0	0.0
66	G	0.0	0.0	0.0	0.0	0.0	0.0
		0.0	0.0	0.0	0.0	0.0	0.0
67	G	-8.256582E-04	0.0	9.708828E-01	0.0	0.0	0.0
		1.956982E-06	0.0	5.097098E-06	0.0	0.0	0.0
68	G	-1.454530E-03	0.0	9.525793E-01	0.0	0.0	0.0
		1.397832E-06	0.0	5.049449E-06	0.0	0.0	0.0
69	G	-1.862047E-03	0.0	9.039381E-01	0.0	0.0	0.0
		9.948490E-07	0.0	4.812719E-06	0.0	0.0	0.0
70	G	-2.028900E-03	0.0	8.303837E-01	0.0	0.0	0.0
		6.911993E-07	0.0	4.424269E-06	0.0	0.0	0.0
71	G	-1.964449E-03	0.0	7.367461E-01	0.0	0.0	0.0
		4.595932E-07	0.0	3.917166E-06	0.0	0.0	0.0
72	G	-1.707455E-03	0.0	6.276297E-01	0.0	0.0	0.0
		2.850667E-07	0.0	3.322441E-06	0.0	0.0	0.0
73	G	-1.306714E-03	0.0	5.074964E-01	0.0	0.0	0.0
		1.583102E-07	0.0	2.669432E-06	0.0	0.0	0.0
74	G	-8.369389E-04	0.0	3.807077E-01	0.0	0.0	0.0
		7.238538E-08	0.0	1.986332E-06	0.0	0.0	0.0
75	G	-4.089163E-04	0.0	2.513338E-01	0.0	0.0	0.0
		2.111750E-08	0.0	1.298597E-06	0.0	0.0	0.0
76	G	-1.075908E-04	0.0	1.232281E-01	0.0	0.0	0.0
		-1.143689E-09	0.0	6.295029E-07	0.0	0.0	0.0
77	G	0.0	0.0	0.0	0.0	0.0	0.0
		0.0	0.0	0.0	0.0	0.0	0.0
78	G	-1.155481E-03	0.0	9.794773E-01	0.0	0.0	0.0
		1.672905E-06	0.0	6.266179E-06	0.0	0.0	0.0
79	G	-2.399936E-03	0.0	9.597895E-01	0.0	0.0	0.0
		1.186606E-06	0.0	6.226535E-06	0.0	0.0	0.0
80	G	-3.117841E-03	0.0	9.090682E-01	0.0	0.0	0.0
		8.382435E-07	0.0	5.933413E-06	0.0	0.0	0.0

COMPLEX EIGENVALUE # -4.299365E 01, 2.438104E 02

COMPLEX EIGENVECTOR NO. 1

%REAL/IMAGINARY<

POINT ID.	TYPE	T1	T2	T3	R1	R2	R3
81	G	-3.398121E-03	0.0	8.333347E-01	0.0	0.0	0.0
		5.776104E-07	0.0	5.444286E-06	0.0	0.0	0.0
82	G	-3.331977E-03	0.0	7.377049E-01	0.0	0.0	0.0
		3.796906E-07	0.0	4.805522E-06	0.0	0.0	0.0
83	G	-3.000228E-03	0.0	6.267658E-01	0.0	0.0	0.0
		2.313700E-07	0.0	4.056881E-06	0.0	0.0	0.0
84	G	-2.429266E-03	0.0	5.051183E-01	0.0	0.0	0.0
		1.247898E-07	0.0	3.238052E-06	0.0	0.0	0.0
85	G	-1.675627E-03	0.0	3.774043E-01	0.0	0.0	0.0
		5.412210E-08	0.0	2.388529E-06	0.0	0.0	0.0
86	G	-8.616298E-04	0.0	2.482576E-01	0.0	0.0	0.0
		1.388743E-08	0.0	1.546768E-06	0.0	0.0	0.0
87	G	-2.602104E-04	0.0	1.211063E-01	0.0	0.0	0.0
		-2.379789E-09	0.0	7.424397E-07	0.0	0.0	0.0
88	G	0.0	0.0	0.0	0.0	0.0	0.0
		0.0	0.0	0.0	0.0	0.0	0.0
89	G	3.140246E-03	0.0	9.923148E-01	0.0	0.0	0.0
		1.293364E-06	0.0	7.279742E-06	0.0	0.0	0.0
90	G	1.045843E-03	0.0	9.687310E-01	0.0	0.0	0.0
		9.155754E-07	0.0	7.209034E-06	0.0	0.0	0.0
91	G	3.647679E-05	0.0	9.149035E-01	0.0	0.0	0.0
		6.495297E-07	0.0	6.851943E-06	0.0	0.0	0.0
92	G	-5.943561E-04	0.0	8.372515E-01	0.0	0.0	0.0
		4.496609E-07	0.0	6.280045E-06	0.0	0.0	0.0
93	G	-1.021113E-03	0.0	7.399248E-01	0.0	0.0	0.0
		2.965974E-07	0.0	5.534296E-06	0.0	0.0	0.0
94	G	-1.292510E-03	0.0	6.273159E-01	0.0	0.0	0.0
		1.805830E-07	0.0	4.659594E-06	0.0	0.0	0.0
95	G	-1.399283E-03	0.0	5.039428E-01	0.0	0.0	0.0
		9.607572E-09	0.0	3.702295E-06	0.0	0.0	0.0
96	G	-1.289683E-03	0.0	3.745281E-01	0.0	0.0	0.0
		3.948328E-08	0.0	2.710136E-06	0.0	0.0	0.0

COMPLEX EIGENVALUE # -4.299365E 01, 2.438104E 02

COMPLEX EIGENVECTOR NO. 1

%REAL/IMAGINARY<

POINT ID.	TYPE	T1	T2	T3	R1	R2	R3
97	G	-8.899940E-04	0.0	2.440561E-01	0.0	0.0	0.0
		7.942024E-09	0.0	1.731771E-06	0.0	0.0	0.0
98	G	-2.198826E-04	0.0	1.184142E-01	0.0	0.0	0.0
		-2.124421E-09	0.0	8.208930E-07	0.0	0.0	0.0
99	G	0.0	0.0	0.0	0.0	0.0	0.0
		0.0	0.0	0.0	0.0	0.0	0.0
100	G	2.562455E-02	0.0	9.999847E-01	0.0	0.0	0.0
		1.037440E-06	0.0	7.984262E-06	0.0	0.0	0.0
101	G	2.130111E-02	0.0	9.709112E-01	0.0	0.0	0.0
		7.709538E-07	0.0	7.859415E-06	0.0	0.0	0.0
102	G	1.815323E-02	0.0	9.173859E-01	0.0	0.0	0.0
		5.761815E-07	0.0	7.487722E-06	0.0	0.0	0.0
103	G	1.550989E-02	0.0	8.405455E-01	0.0	0.0	0.0
		4.256486E-07	0.0	6.877421E-06	0.0	0.0	0.0
104	G	1.298229E-02	0.0	7.444139E-01	0.0	0.0	0.0
		3.056070E-07	0.0	6.075591E-06	0.0	0.0	0.0
105	G	1.033797E-02	0.0	6.330148E-01	0.0	0.0	0.0
		2.093842E-07	0.0	5.129852E-06	0.0	0.0	0.0
106	G	7.501367E-03	0.0	5.104108E-01	0.0	0.0	0.0
		1.298604E-07	0.0	4.088665E-06	0.0	0.0	0.0
107	G	4.560426E-03	0.0	3.807074E-01	0.0	0.0	0.0
		6.821460E-08	0.0	3.000698E-06	0.0	0.0	0.0
108	G	1.812001E-03	0.0	2.481658E-01	0.0	0.0	0.0
		2.357728E-08	0.0	1.914841E-06	0.0	0.0	0.0
109	G	-7.490840E-05	0.0	1.174517E-01	0.0	0.0	0.0
		-1.109879E-09	0.0	8.811287E-07	0.0	0.0	0.0
110	G	0.0	0.0	0.0	0.0	0.0	0.0
		0.0	0.0	0.0	0.0	0.0	0.0
111	G	1.218929E-01	0.0	9.805125E-01	0.0	0.0	0.0
		1.620439E-06	0.0	8.149491E-06	0.0	0.0	0.0
112	G	1.008025E-01	0.0	9.631476E-01	0.0	0.0	0.0
		1.281400E-06	0.0	8.202421E-06	0.0	0.0	0.0

COMPLEX EIGENVALUE # -4.299365E 01, 2.438104E 02

COMPLEX EIGENVECTOR NO. 1

%REAL/IMAGINARY<

POINT ID.	TYPE	T1	T2	T3	R1	R2	R3
113	G	8.555585E-02	0.0	9.144474E-01	0.0	0.0	0.0
		1.030063E-06	0.0	7.869553E-06	0.0	0.0	0.0
114	G	7.362384E-02	0.0	8.434644E-01	0.0	0.0	0.0
		8.355046E-07	0.0	7.280154E-06	0.0	0.0	0.0
115	G	6.309545E-02	0.0	7.545364E-01	0.0	0.0	0.0
		6.742798E-07	0.0	6.494103E-06	0.0	0.0	0.0
116	G	5.282794E-02	0.0	6.511770E-01	0.0	0.0	0.0
		5.326319E-07	0.0	5.559921E-06	0.0	0.0	0.0
117	G	4.217869E-02	0.0	5.365651E-01	0.0	0.0	0.0
		4.026728E-07	0.0	4.522720E-06	0.0	0.0	0.0
118	G	3.089698E-02	0.0	4.135290E-01	0.0	0.0	0.0
		2.805867E-07	0.0	3.424676E-06	0.0	0.0	0.0
119	G	1.915073E-02	0.0	2.841530E-01	0.0	0.0	0.0
		1.662643E-07	0.0	2.301465E-06	0.0	0.0	0.0
120	G	7.735681E-03	0.0	1.488102E-01	0.0	0.0	0.0
		6.454121E-08	0.0	1.174074E-06	0.0	0.0	0.0
121	G	0.0	0.0	0.0	0.0	0.0	0.0
		0.0	0.0	0.0	0.0	0.0	0.0

APPENDIX C

SRB SEGMENT TEST REQUIREMENTS

APPENDIX C

TITLE: SRB Segment Test Requirements

1.0 PURPOSE

The purpose of conducting tests on segments of the SRB is to evaluate the analysis of propellant modes.

2.0 OBJECTIVE

The objective of the segment tests is to determine the resonant frequencies, deflection responses, mode shapes and stress distribution in the first two longitudinal axisymmetric thickness shear modes at several burn times.

3.0 TEST SPECIMEN REQUIREMENTS

The test segment shall be fabricated from a typical motor segment case. The dynamic properties of the propellant shall be identical to the SRB operational propellant. Grain design including liner and flap design shall be representative of actual SRB flight hardware at a forward segment representative of the smallest bore diameter.

The length of the segment shall be approximately 300 inch. If SRB operational segment length is less than 300 inch, it shall determine the length of the test segment.

The propellant shall be configured to several different bore diameters repre sentative of motor segment conditions or burn times as follows:

1) Preignition

2) Fundamental acoustic combustion resonance equal to fundamental longitudinal shear

3) A bore diameter which yields the highest strains (See Section 4. 4. 3)

4.0 TEST ENVIRONMENT

The vibratory excitation shall be sinusoidal sweep. The test frequency range shall be 10 to 50 Hertz. The sweep rate shall be one octave per minute.

Vibratory excitation forces shall be applied longitudinally to the motor segment case at the fore and aft interface. The forces shall be uniformily distributed at the case/exciter interface. The net force at each interface shall be equal in magnitude, in phase and sufficient to cause (1) a 1g peak sinusoidal acceleration and (2) an excitation equal to the maximum expected levels at the interfaces for each burn time.

The test segment shall be maintained at a uniform ambient temperature for a sufficient time prior to starting test so that a uniform temperature through-out the segment is obtained. This same ambient temperature shall be maintained during the test.

5.0 INSTRUMENTATION

Test input and response vibration levels shall be measured with accelerometers. A sufficient number of accelerometers shall be placed on the fore and aft motor case interfaces to monitor the motion. Accelerometers shall also be attached to the surface and embedded within the propellant to evaluate the fundamental mode shape through-out a cross-section formed by the longitudinal axis and radius vector. Measurements shall be made at grid points formed by radii and longitudinal lines within the plane.

Strain gage measurements shall be made at the same grid point measurements defined for accelerometers so that the strain distribution can be evaluated.

6.0 DATE REQUIREMENTS

Data shall be taken during each test to insure that frequency response, mode shapes, acceleration and strain levels can be evaluated.

References and Bibliography

The bibliography consists of two sections. Section 1 contains those references which were found to be very useful. These references are abstracted for future reference. Section 2 contains those references which were used, but not considered as applicable as the references in Section 1.

Section 1.

1. Achenbach, J. D.: "Axial Shear Vibrations of a Cylinder of Decreasing Thickness," AIAA Journal, Vol. 4, No. 7, pp. 1233-1240, July 1966.

This paper presents an analytical study of the axial shear vibrations of a long hollow cylinder that is subjected to time-dependent body forces in the axial direction. The outer surface of the cylinder is bonded to a rigid case, and the inner radius increases monotonically with time. An expression is determined for the shear stress at the bond interface. It is shown that the instantaneous frequency of the shear bond stress increases, and that its amplitude decreases toward burnout time. The axial shear vibrations of an ablating viscoelastic cylinder are discussed briefly .

2. Anon.: "Final Report Frequency Investigation of the TU-122-1511.11 Minuteman Motor," TR Thiokol Chemical Corporation.

This report investigates the input to the first stage Minuteman motor during transportation. The critical speed was determined for traversing road course with different height boards.

3. Anon.: "Final Report Resonance Search and Response Test Stage 1 Minuteman Motor with Embedded Instrumentation (TU-122-1834.1062, TTM 009), TR Thiokol Chemical Corporation.

4. Anon: "Final Report Resonance Search Stage 1 Minuteman Motor (TU-122-1834.633; TTM-010)" TR Thiokol Chemical Corporation.

These test reports identified the resonant frequencies of the first stage Minuteman motor which could be excited during transportation and handling. The frequencies identified were the coupled thickness shear mode, the lobar mode, and lateral bending modes. Also identified were the resonant frequencies of the dome and nozzle. Responses were measured at the various resonances with embedded instrumentation.

5. Anon.: "Ground Dynamic Tests (WS-133A)", Test No. T2-1704, Boeing Airplane Company, Seattle, Washington, January 1961.

Tests were conducted on a full-scale Minuteman missile, containing inert propellant, to determine structural dynamic characteristics of the airborne vehicle.

Objectives of the Test were:

1. To define modal characteristics (frequencies, mode shapes and damping);

2. To obtain slope measurements at anticipated flight control sensor locations;

3. To monitor auxiliary equipment resonances;

4. To measure the missile's response to a lateral thrust component, simulated by a sinusoidal force applied at the nozzle hinge.

6. Baltrukonis, J. H. and Gottenberg, W. G.: "Thickness-Shear Vibrations of Circular Bars," Space Technology Laboratories, Inc. Report No. GM-TR-0165-00518, Nov. 1958.

Exact general solutions of the three-dimensional elasticity equations of motion in polar cylindrical coordinates are obtained for axisymmetric and antisymmetric thickness-shear vibrations. These solutions are applied in solving five solid and hollow circular bar problems. Natural frequencies are tabulated and mode shapes are plotted.

7. Baltrukonis, J. H.: "A Survey of Structural Dynamics of Solid Propellant Rocket Motors," NASA CR-658, Dec. 1966.

In the paper a survey of the dynamic problems of solid propellant rocket motors is presented starting from the simplest model thereof and proceeding, step-by-step, to the consideration of more sophisticated and realistic models. The consideration is restricted to infinitesimal deformations of propellant grains with linear mechanical properties. Substantial progress has been achieved towards the solution of many important dynamical problems. Pertinent developments are summarized and indications are made along which lines future study should proceed. A few illustrative solutions are included in areas wherein progress has been substantial.

8. Baltrukonis, J. H.; Gottenberg, W. G.; and Schreiner, R. N.: "Axial-Shear Vibrations of an Infinitely Long Composite Circular Cylinder," J. Acoust. Soc. AM., Vol. 33, No. 11, Nov. 1961, pp. 1447-1457.

Exact general solutions of the three-dimensional elasticity equations of motion in polar cylindrical coordinates are written for axisymmetric axial-shear vibrations. The frequency equation follows immediately from the boundary conditions for the problem of the infinitely long, composite cylinder with two concentric circular-cylindrical layers which are perfectly bonded at their interface. The branches of the frequency equation are plotted and analyzed. The conditions are pointed out under which it is possible to obtain reasonably accurate estimates of the natural frequencies by assuming that the motions of the casing and core are uncoupled.

9. Beyer, E. B.: "Nonlinear Mechanical Behavior of Solid Propellants," AIAA Paper No. 65-159.

The mechanical response of standard solid propellants was studied by extensive analysis of data measured under conditions of constant strain rate, constant strain, and dynamic shear strain. Nonlinear viscoelasticity has been found to occur when propellant samples are strained beyond a few tenths of one percent by tensile test methods currently used by most investigators. Studies conducted over a wide range of strain rates (10^7 to 10 min^{-1}) indicate that nonlinearity can occur (1) by loss of reinforcement due to dewetting and (2) by the "Mullins Effect" in a matrix with chemical adhesive bonding between binder and filler. In case (1) dewetting was observed to depend only on the applied stress and the temperature. The linear viscoelastic response obtained from small constant strain rate and dynamic data differed from the constant strain (2 to 5 percent) stress-relaxation modulus by as much as an order of magnitude. At very low strain rates equilibrium behavior was obtained up to strains as high as 7 percent. The time and temperature dependence of both the reinforced and non-reinforced modulus is discussed and related to long term ambient tests and actual motor behavior.

10. CPIA Publication No. 21: "Solid Propellant Mechanical Behavior Manual."

This document is a general information reference on mechanical properties of solid propellants. It covers mechanics of viscoelasticity, failure criteria, procedures for physical characterization, strain measurement techniques nomenclature, symbology, surveillance for reliability and aging, crosslink density and equilibrium stress-strain measurements.

11. CPIA Publication No. 214: "Handbook for the Engineering Structural Analysis of Solid Propellants," Prepared by Fitzgerald, J. E. and Hufferd, W. L., May 1971.

This Handbook represents an attempt to present an accurate report and evaluation of the current state-of-the-art of solid propellant grain structural integrity. Major emphasis is given to the requirements for meaningful material characterization, structural analysis and failure analysis of solid propellants. The Handbook has been written primarily for the designer/analyst.

12. Davey, A. B. and Payne, A. R.: Rubber in Engineering Practice, Palmerton Publishing Co., Inc., New York, 1964.

This text describes the behavior of rubber under rapidly changing stresses such as vibrations and shocks, and of the dependence of this behavior on such factors as temperature, frequency and rate of deformation, as well as shape and environment. Of particular importance is the sections on "dynamics" properties of rubber and methods of measuring them.

13. Gottenberg, W. G.: "Results of Minuteman Engine Associate Contractors Round Robin Propellant Mechanical Properties Test", STL Report, 6121-7244-KU000, July 26, 1963.

Values of stress relaxation and dynamic modulus as measured by Aerojet General Corporation, Hercules Powder Co., Thiokol Chemical Corp., and Space Technology Labs are compared to show the dispersion of data.

14. Kingsbury, H. B.; Vinson, J. R.; and Soler, A. I.: "On the Lobar and Longitudinal Vibrations of Solid Propellant Rocket Motors", AIAA Paper No. 65-172.

Approximate analytical methods are developed to determine the lobar (breathing) mode shapes and natural frequencies of a solid propellant motor, the axially symmetric propellant mode shapes and natural frequencies during longitudinal vibration, and the propellant stresses during forced longitudinal vibration. For lobar vibrations, general expressions for both kinetic energy and strain energy are formulated utilizing a plane strain solution of the motor undergoing arbitrary inextensional deformations of the case. Employing a variational technique, analytical expressions for the lobar frequencies and mode shapes are determined. For longitudinal vibrations, the propellant is considered as a thick, hollow, elastic, finite cylinder. Functional forms for stresses and displacements are assumed with arbitrary radial and axial dependence. The repeated use of Reissner's Principle yields equations applicable to various boundary conditions. From these, natural frequencies and mode shapes are determined.

15. Kruse, R. B.: "Laboratory Characterization of Solid Propellant Mechanical Properties," AIAA Paper, No. 65-147.

This paper surveys the development of techniques for the laboratory testing of solid propellants, reviews the results to date in regard to to the degree of understanding they provide about the nature of these materials, and indicates briefly the direction of f uture work in this area.

16. NASA SP-8064: "Solid Propellant Selection and Characterization"

The purpose of this monograph is to organize and present, for effective use in design, the significant experience and knowledge accumulated in development and operational programs to date. It reviews and assesses current design practices, and from them establishes firm guidance for achieving greater consistency in design, increased reliability in the end product, and greater efficiency in the design effort.

17. Nielsen, L. E.: Mechanical Properties of Polymers, Reinhold Publishing Corporation, New York, 1962.

This text presents a concise review of a wide variety of mechanical properties of high polymers from both the theoretical and experimental viewpoints. Of particular importance are the discussions on the time temperature superposition principle, models of viscoelastic theory, and interrelation ships between various properties.

18. Stibor, G.S.: Working Papers

A study was conducted to investigate the structural dynamics of a solid rocket motor and attachment structure. The discussion and results of the study which follows consists of the following: structural resonant frequencies of the motor and motor with attachments; motor chamber acoustic modes (self-generated vibration environment); and vibration data from previous static tests of 156-inch diameter solid rocket motors.

19. Williams, M. L.: "Structural Analysis of Viscoelastic Materials," AIAA J., 2, 785-804, 1964.

This paper discusses the material characterization, engineering analysis, and failure criteria of viscoelastic materials. Of particular importance is the material characterization where different mathematical models are used to explain the behavior of viscoelastic material.

20. Williams, M. L.; Landel, R. F.; and Ferry, J. D.: "The Temperature Dependence of Relaxation Mechanisms in Amorphous Polymers and Other Glass-Forming Liquids," J. AM. Chem. Soc., 77, p. 3701, 1955.

The temperature dependence of stress relaxation of polymers is studied. Data taken at different temperatures can be shifted on the time scale to obtain relaxation data over broad time periods.

Section 2.

21. Achenbach, J. D.: "Dynamic Response of a Long Case-Bonded Viscoelastic Cylinder," AIAA Jorunal, Vol. 3, No. 4, pp. 673-677, April 1965.

22. Achenbach, J. D.: "Dynamic Response of an Encased Elastic Cylinder with Ablating Inner Surface," AIAA Journal, Vol. 3, No. 6, pp. 1142-1144, June 1965.

23. Achenbach, J. D.: "Thickness Shear Vibrations of an Ablating Rocket," TR No. 65-3, Northwestern University, July 1965.

24. Achenbach, J. D.: "Forced Vibrations of a Burning Rocket," AIAA Journal, Vol, 3, No. 7, pp. 1333-1336, July 1965.

25. Achenbach, J. D.: "Dynamic Response of a Viscoelastic Cylinder with Ablating Inner Surface," Northwestern University TR No. 65-6, Dec. 1965.

26. Achenbach, J. D. and Herrmann, G.: "Forced Motions of an Encased Cylinder of Decreasing Thickness," J. Acoust. Soc. AM., Vol. 39, No. 6, pp. 1145-1153, June 1966.

27. Alfrey, T.: "Non-Homogeneous Stresses in Viscoelastic Media," Q. Appl. Math., Vol. 2, pp. 113-119, July 1944.

28. Anderson, McKay: "Case Bond Stress Calculations for Flapped Cylindrical Analogs of Solid Propellant Rocket Motors," AFRPL-TR-72-55, AD 744901.

29. Anderson, J. M. and Durrant, S. O.: "A Finite-Element Solution for Acoustic Mode Shapes and Frequencies in Rocket Motor Combustion Cavities," Unpublished Report, Hercules Incorporated.

30. Anon: Aerospace Metals Handbook, Vol. I, "Ferrous Alloys," Code 1213, March 1966.

C-2

31. Anon.: "Fracture Toughess (FZM-12-408)" General Dynamics Corporation, Fortworth

32. Baltrukonis, J. H. and Gottenberg, W. G.: "Transverse Wave Propagation in a Solid, Elastic Mass Contained by an Infinitely Long, Rigid, Circular-Cylindrical Tank," Presented at the Fourth Midwestern Conference on Solid Mechanics, Sept. 1959.

33. Baltrukonis, J. H.; Gottenberg, W. G.: "Thickness-Shear Vibrations of Circular Bars," J. Acoust. Soc. AM., Vol. 31, No. 6, June 1959, pp. 734-739.

34. Baltrukonis, J. H.; Gottenberg, W. G.; and Schreiner, R. H.: "The Dynamic Response of a Finite Rigid Mass Concentrically Carried by a Viscoelastic Disk," Proc. Fourth U.S. National Congress of Applied Mechanics, 867 (1962).

35. Baltrukonis, J. H.; Gottenberg, W. G.; and Schreiner, R. H.: "Transverse Wave Propagation in a Hollow, Incompressible, Elastic Mass Contained by an Infinitely Long, Rigid, Circular-Cylindrical Tank," Space Technology Laboratories, Inc. Report No. TR-59-0000-00865, Oct. 1959.

36. Baltrukonis, J. H.; Gottenberg, W. G.; and Schreiner, R. N.: "Dynamics of a Hollow, Elastic Cylinder Contained by an Infinitely Long Rigid Circular-Cylindrical Tank," J. Acoust Soc. AM., Vol. 32, No. 12, Dec. 1960, pp. 1539-1546.

37. Baltrukonis, J. H.; Gottenberg, W. G.; and Schreiner, R. N.: "Solution and Experimental Results for a Problem in Linear Viscoelasticity," Trans. Soc. Rheol., VI, 41-60 (1962).

38. Bergman, G. H. and Jessen, E. C.: "Evaluation of Conventional Rocket Motor Instrumentation for Analysis of Oscillatory Combustion."

39. Bird, J. F.; Hart, R. W.; and McClure, F. T.: "Vibrations of Thick-Walled Hollow Cylinders: Exact Numerical Solutions," J. Acoust. Soc. AM., Vol. 32, No. 11, Nov. 1960, pp. 1404-1412.

40. Bird, J. F.: "Vibrations of Thick-Walled Hollow Cylinders: Approximate Theory," J. Acoust. Soc. AM., Vol. 32, No. 11, Nov. 1960, pp. 1413-1419.

41. Brull, M. A.; Kingbury, H. B.; and Vinson, J. R.: "On the Flexural Vibrations of Solid Propellant Rocket Motors," Presented at AIAA Launch and Space Vehicle Shell Structures Conference, April 1-3, 1963.

42. Buchdahl, R. and Nielsen, L. E.: "The Application of Nutting's Equation to the Viscoelastic Behavior of Certain Polymeric Systems," J. App. Phy., Vol. 22, No. 11, p. 1344, Nov. 1951.

43. Craig, P. S. and Sforzini, R. H.: "Materials and Processes for a 156-Inch Diameter Monolithic Motor," AIAA Paper No. 65-164.

44. Felix, B. R.; Lefebure, C. A.; and Tyson, M. R.: "Titan III Solid Motor System Integration," AIAA Paper No. 65-153.

45. Flippin, L. G.; Gammell, L. W.; and Stibor, G. S.: "Resonance Frequency of Large Solid Propellant Rocket Motor Determined by Mechanical Impedance," The Shock and Vibration Bulletin, Bulletin 34, Part 3, pp. 59-73, Dec. 1964.

46. Francis, E. C. and Carlton, C. H.: "Some Aspects of Nonlinear Mechanical Behavior of a Composite Propellant," J. Spacecraft Rockets, Vol. 6, No. 1, Jan. 1969, p. 65.

47. Gilmore, R. T.: "Vibration and Frequency Response of Minuteman I Stage", Thiokol Chemical Corporation Memo.

48. Henry, L. A. and Freudenthal, A. M.: "Forced Vibrations of a Finite Viscoelastic Cylinder Case-Bonded to a Thin Shell", AIAA Paper No. 65-173.

49. Herting, D. N.; Joseph, J. A.; Kuusinen, L. R.; and Macneal, R. H.: "Acoustic Analysis of Solid Rocket Motor Cavities by a Finite Element Method".

50. Jaszlics, I. J. and Morosow, G.: "Dynamic Testing of a 20% Scale Model of the Titan III", AIAA Syposium on Structural Dynamics and Aerogalsticity, Aug-Sept. 1965, pp. 477-485.

51. Langhaar, H. L.: Dimensional Analysis and Theory of Models, John Wiley and Sons Inc., New York, 1965.

52. Lee, E. H.: "Inhibition of Fracturing in Encased Solid Propellant Grains", ARS Journal, June 1962, p. 913-916.

53. Lee, E. H. and Rogers, T. G.: "Solution of Viscoelastic Stress Analysis Problems Using Measured Creep or Relaxation Functions", J. Applied Mechanics, 30, 127 (March 1963).

54. Lindsey, G. H.; and Williams, M. L.: "Structural Integrity of an Ablating Rocket Subject to Axial Acceleration," AIAA Journal, Vol. 3, No. 2, pp. 258-262, Feb. 1965.

55. Marsh, H. E. and Udlock, D. E.: "Formulating Propellants for Fully Case-Bonded End-Burning Motors".

56. Miles, D. O.: "Sinusoidal Shear Generator for Study of Viscoelasticity", J. Applied Physics, Vol. 33, No. 4, April 1961, pp. 1422-1428.

57. Mixson, J. S.; Morgan, H. G.; Runyan, H. L.: "Role of Dynamic Models in Launch Vehicle Development", Presented at a Colloquium on Experimental Techniques in Shock and Vibration at the Winter Annual Meeting of the ASME, New York, New York, November 27, 1962.

58. NASA CR-936: "Dynamic Stability of Space Vehicles", Vol. I - Lateral Vibration Modes by G. B. Paddock Vol. II - Determination of Longitudinal Vibration Modes by J. A. Staley.

59. NASA CR-1449: "Non-Linear Longitudinal Dynamics of an Orbital Lifting Vehicle", by Nguyen X. Vinh and Arthur J. Dobrzelecki, Oct. 1969.

60. NASA SP-8012: "Natural Vibration Modal Analysis", Sept. 1968.

61. NASA SP-8025: "Solid Rocket Motor Metal Cases", April 1970.

62. NASA SP-8050: "Structural Vibration Prediction", June 1970.

63. NASA SP-8075: "Solid Propellant Processing Factors in Rocket Motor Design".

64. NASA SP-8076: "Solid Propellant Grain Design and Internal Ballistics".

65. NASA TN D-5778: "Lateral Vibration Characteristics of the 1/10-Scale Apollo/Saturn V Replica Model", April 1970.

66. NASA TN D-5831: "Application of Analysis and Models to Structural Dynamic Problems Related to the Apollo-Saturn V Launch Vehicle", June 1970.

67. Nashif, A. D. and Nichols, T.: "Attenuation of Vibrational Amplitudes through the Use of Multiple-Layered Damping Treatments", Presented at the Vibrations Conference and the International Design Automation Conference, Sept. 8-10, 1971, Toronto, Canada.

68. Nelson, J. M.; Cook, W. A.; and Stibor, G. S.: "Three-Dimensional Photoelastic and Finite-Element Analysis of a Propellant Grain," Experimental Mechanics, Vol. 12, No. 9, pp. 436-440, Sept. 1972.

69. Painter, G. W.: "Dynamic Properties of BTR Elastomer", Presented at SAE National Aeronautic Meeting, Los Angeles, California, Sept. 29-Oct. 4, 1958.

70. Sampson, R. G. and Peters, A. P.: "Status Report on 120-Inch Motor Design and Development", AIAA Paper No. 65-163.

71. Sayer, L. and Stibor, G.: "Program Plan for Poseidon C3 First Stage Motor Oscillations", PC3-69-196, 4 May 1970, Unpublished Report.

72. Smith, T. L.: "Approximate Equations for Interconverting the Various Mechanical Properties of Linear Viscoelastic Materials", Trans. Soc. Rheol. II, 131-151 (1958).

73. Smith, J. L.: "Nonlinear Viscoelastic Response of Amorphous Elastomers to Constant Strain Rates", Trans. Soc. Rheol., VI, 61-80 (1962).

74. Smith, T. L.: "Stress-Strain-Time-Temperature Relationships for Polymers, "Special Tech Publication 325, American Society for Testing Materials (1962).

75. Steyer, Carl C.: "Analysis of a Thick-Walled Layered Anisotropic Elastic Cylinder Subjected to a Radial Pressure Utilizing Three-Dimensional Material Properties", AIAA Paper No. 65-174.

76. Stibor, G. S.: "Poseidon C3 First Stage Motor Acoustic Studies Simulation and Analysis of Observed Static Test Phenomena," PC3-70-227, 24 August 1970, Unpublished Report.

77. Sun, C. L.; Yu, Yen; and Evan-Iwanowski, R. M.: "Non-stationary Responses of Cylindrical Shells Near Parametric Resonances" Developments In Mechanics, Vol. 6, Proceedings of the 12th Midwestern Mechanics, Conference: 68.

78. Tormey, J. F. and Britton, S. C.: "Effect of Cyclic Loading on Solid Propellant Grain Structures", AIAA J., Vol. 1, No. 8, August 1963.

79. Wagner, F. R.: "Solid Load Definition Study: The Vibration Environment", UTEC DO 68-055 or AFRPL TR-68-140, Jan. 1969.

80. Williams, F. A.; Barrere, M.; and Huang, N. C.: Fundamental Aspects of Solid Propellant Rockets. England, Technivision Services, 1969, Agardograph 116.

81. Williams, M. L., "Mechanical Properties and the Design of Solid Propellant Motors," ARS Progress In Astronautics and Rocketry: Solid Propellant Rocket Research, Ed. By Martin Summerfield (Academic Press, New York, 1960), Vol 1, p. 67.

82. Zienkiewicz, D. C.; Watson, M.; and King, I. P.: "A Numerical Method of Viscoelastic Stress Analysis", INT, J. Mech. SCI., Pergamon Press, 1968, Vol. 10, pp. 807-827.